JGR Atmospheres

RESEARCH ARTICLE
10.1029/2024JD043124

The First Firn Core From the Cordillera Darwin Icefield: Implications for Future Ice Core Research

Dieter R. Tetzner[1], Elizabeth R. Thomas[1], Claire S. Allen[1], Robert D. McCulloch[2], Bianca B. Perren[1], Amy McGuire[3], Delia Segato[4,5,6], Franziska Temme[7], Johannes J. Fürst[7], Dorothea Moser[1,8], Francisco Fernandoy[9], Camilo Rada[10], Jack Humby[1], and Shaun Miller[1]

[1]British Antarctic Survey, Cambridge, UK, [2]School of GeoSciences, The University of Edinburgh, Edinburgh, UK, [3]School of Earth and Environment, Faculty of Environment, University of Leeds, Leeds, UK, [4]Department of Environmental Sciences, Informatics and Statistics, Ca' Foscari University of Venice, Venezia-Mestre, Italy, [5]CNR-Institute of Polar Sciences, Venezia-Mestre, Italy, [6]Currently at Joint Research Center, European Commission, Ispra, Italy, [7]Institut für Geographie, Friedrich-Alexander-Universität Erlangen-Nürnberg, Erlangen, Germany, [8]Department of Earth Sciences, University of Cambridge, Cambridge, UK, [9]Laboratorio de Análisis Isotópico, Facultad de Ingeniería, Universidad Andrés Bello, Viña del Mar, Chile, [10]CIGA, Centro de Investigación Gaia Antártica, Universidad de Magallanes, Punta Arenas, Chile

Key Points:

- Surface air temperature estimations suggest the Cordillera Darwin Icefield (CDI) has been progressively exposed to surface melt conditions
- Firn core layers present minor post-depositional disruptions, preserving the original seasonality of locally sourced impurities
- High-elevation sites (>2,000 m a.s.l) in the CDI have the potential to hold valuable paleoenvironmental records

Supporting Information:

Supporting Information may be found in the online version of this article.

Correspondence to:

D. R. Tetzner,
dietet95@bas.ac.uk

Citation:

Tetzner, D. R., Thomas, E. R., Allen, C. S., McCulloch, R. D., Perren, B. B., McGuire, A., et al. (2025). The first firn core from the Cordillera Darwin Icefield: Implications for future ice core research. *Journal of Geophysical Research: Atmospheres*, *130*, e2024JD043124. https://doi.org/10.1029/2024JD043124

Received 17 DEC 2024
Accepted 14 APR 2025

Author Contributions:

Conceptualization: Dieter R. Tetzner, Elizabeth R. Thomas, Claire S. Allen
Data curation: Dieter R. Tetzner
Formal analysis: Dieter R. Tetzner, Elizabeth R. Thomas, Claire S. Allen, Robert D. McCulloch, Bianca B. Perren, Amy McGuire, Delia Segato, Franziska Temme, Johannes J. Fürst, Dorothea Moser
Funding acquisition: Dieter R. Tetzner
Investigation: Dieter R. Tetzner, Elizabeth R. Thomas, Claire S. Allen, Robert D. McCulloch, Bianca B. Perren, Amy McGuire, Delia Segato, Franziska Temme, Johannes J. Fürst, Dorothea Moser, Francisco Fernandoy, Camilo Rada, Jack Humby, Shaun Miller

Abstract The Southern Hemisphere westerly winds (SHWWs) (45–65°S) are important regulators of the Southern Hemisphere climate. The scarcity of observational records at the core of the wind belt hinders our understanding of the environmental impact and long-term variability of the westerly winds. The Cordillera Darwin Icefield (CDI) (54–55°S) is favorably located to capture environmental changes at the current core of the SHWW belt. Here, we present chemical and microparticle records from the first firn core from the CDI. We evaluate regional climate reanalysis data using in situ automatic weather station observations and apply a downscaling approach to study regional-to-local environmental conditions at the firn core site. We use these records to assess the preservation of local-to-regional environmental information in the firn. Our CDI firn core records present minor post-depositional disruptions, preserving the original seasonality of locally sourced impurities. Local surface air temperature and melt estimations suggest the icefield has been progressively exposed to surface melt conditions, but not enough to produce significant melt at the firn core site. Air mass trajectories demonstrate air parcels are directly transported from local marine and terrestrial environments, establishing a route for the transport and deposition of chemical compounds and aerosols to the firn core site. These results highlight the potential of high elevation sites (>2,000 m a.s.l) in the CDI to hold valuable paleoenvironmental records directly from the core of the SHWW belt, records which are currently threatened by increasing surface air temperatures.

Plain Language Summary Westerly winds over the Southern Ocean play a crucial role in regulating the climate of the Southern Hemisphere. The lack of meteorological records makes it difficult to understand how these winds have changed over time. Without direct meteorological observations, natural climate archives, such as ice, can provide insights into past wind changes. The Cordillera Darwin icefield, located in the southernmost tip of South America, is well-positioned to record changes in the westerly winds. Here, we present results from the first firn core drilled from this icefield and include the sparse regional meteorological data to assess the preservation of local-to-regional environmental information in the firn. Our firn core record presents minor disruptions and so preserves the seasonal cycles of inputs of impurities. Air transport models demonstrate air masses reaching the firn core site are directly transported from local marine and terrestrial environments, establishing a route for the transport of impurities. Air temperature and surface melt estimations suggest the icefield has been progressively exposed, although not enough to cause significant melt at the firn core site. These results highlight the potential of high-elevation sites (>2,000 m.a.s.l) in this icefield to hold valuable westerly wind records, although currently threatened by increasing air temperatures.

1. Introduction

The Southern Hemisphere westerly winds (SHWWs) (45–65°S) are fundamental in the climate system, in part, because of their strong imprint in Southern Ocean circulation, regulating the oceanic uptake of heat and carbon dioxide (Le Queré et al., 2007; Lovenduski et al., 2007; Russell et al., 2006). Over the past few decades, the core of the SHWWs has been strengthening and migrating south (Fogt & Marshall, 2020; Marshall, 2003), likely in

Methodology: Dieter R. Tetzner, Elizabeth R. Thomas, Claire S. Allen
Resources: Jack Humby, Shaun Miller
Validation: Elizabeth R. Thomas, Claire S. Allen, Robert D. McCulloch, Bianca B. Perren
Writing – original draft: Dieter R. Tetzner
Writing – review & editing: Dieter R. Tetzner, Elizabeth R. Thomas, Claire S. Allen, Robert D. McCulloch, Bianca B. Perren, Amy McGuire, Delia Segato, Franziska Temme, Johannes J. Fürst, Dorothea Moser, Francisco Fernandoy, Camilo Rada

response to the anthropogenic increase in greenhouse gas emissions and stratospheric ozone depletion (Cai & Cowan, 2007; Deng et al., 2022; Gillett & Thompson, 2003; Polvani et al., 2011; Son et al., 2008). It has been proposed that these SHWW deviations are responsible for shifting the main moisture-carrying storm tracks south (away from mid-latitude continental landmasses), causing increased snowfall and surface air temperature warming in West Antarctica and the Antarctic Peninsula, while promoting glacier thinning and retreat, as well as instigating droughts and wildfires in Patagonia (Gorodetskaya et al., 2023; Holz & Veblen, 2011; Marshall et al., 2017; Minowa et al., 2023; Möller et al., 2007; Wachter et al., 2020). Instrumental SHWWs data sets are short and scarce, with only a few records extending beyond the satellite-era (pre-1979) (Fogt & Marshall, 2020). The lack of longer-term SHWWs records presents a major challenge in assessing the historical context of the recently observed changes.

The Patagonia region provides an ideal geographical setting to study changes in the SHWW belt as it is the only continuous landmass that extends to 56°S (Björck et al., 2012; Holz & Veblen, 2011; Kilian & Lamy, 2012; Moreno et al., 2012, 2014; Van Daele et al., 2016; Xia et al., 2018 and references therein), providing a latitudinal bridge between low and high latitudes. However, seasonal to annual resolution climate archives from Patagonia are scarce, and very few paleo records capture environmental changes during the last century (Kilian & Lamy, 2012 and references therein). This limits our ability to explore environmental changes prior to the observational period or produce a detailed regional assessment of the recent changes.

Layers of snow, compacted into firn and accumulated over the years, preserve a broad and detailed record of environmental conditions at approximately the time snow fell over the surface, making firn/ice cores faithful recorders of highly resolved paleoenvironmental information (Alley, 2010). Only three ice cores have been drilled within the core of the SHWW belt, one 14-m firn core from Bouvet Island (Thomas et al., 2021) and two 1-m long ice cores from a glacier terminal margin in South Georgia Island (Mayewski et al., 2016) (Figure 1). Despite these records being obtained from the core of the SHWWs, Bouvet and South Georgia islands are over 2,000 and 4,500 km East from Patagonia, respectively, and represent very different settings to the Patagonia-Antarctic latitudinal transect. Firn cores have been previously retrieved from the Patagonian Icefields (Aristarain & Delmas, 1993; Kohshima et al., 2002; Matsuoka & Naruse, 1999; Schwikowski et al., 2006, 2013; Vimeux et al., 2008; Yamada, 1987) and from the northern Antarctic Peninsula (Fernandoy et al., 2018; Hoffmann-Abdi et al., 2023; Jiahong et al., 1998; Simoes et al., 2004), at the current north and south margin of the SHWW belt, respectively (Figure 1). To date, no cores have been obtained from the core of the SHWW belt in the South American sector, creating a 1,600 km latitudinal data gap.

The Cordillera Darwin Icefield (CDI) (54.5–55°S; 69–70.5°W) is located in the southernmost mountain range in the South American Andes, directly in the path of the SHWW belt (Figure 1). Moisture-carrying storm tracks transported by the SHWW belt impact the steep Cordillera Darwin mountain range, leading to orographically induced precipitation and the formation of large glaciers. The CDI is formed by over 600 glaciers, some extending from CDI's highest peak, Mount Shipton (2,470 m a.s.l.) to sea level. The Cordillera Darwin steep topography supports the development of glaciers at relatively high elevations (>2,000 m above sea level (a.s.l.)), a geographic condition which is almost unique within the 53–63°S latitudinal band. CDI's margins are characterized by the presence of dense deciduous and evergreen forest and fjords transitioning to steppe and cool semi-desert to the north (Barrera et al., 2000; Markgraf & Huber, 2010; Vidal et al., 2023), terrain which has historically hindered access and prevented widespread exploration of the CDI. Despite its southern location, the region experiences austral summer heatwaves (González-Reyes et al., 2023), potentially causing surface melting of glaciers up to relatively high elevations. A recent field study, focused on CDI's fresh snow composition, reported the presence of considerable surface melt in CDI, at 1,800 m a.s.l, potentially threatening environmental records preserved in CDI firn (Mayewski et al., 2016). However, the high-elevation areas of the CDI (>2,000 m a.s.l.) might still provide suitable conditions for preserving environmental records. In 2020, as part of the National Geographic Cordillera Darwin Ice CorE Survey (CODICES) project, the first-ever firn core was drilled on the CDI, providing an unprecedented opportunity to evaluate the quality of environmental records in CDI firn.

In this study, we evaluate the preservation of chemical and microparticle records in our firn core from the CDI. Physical firn properties, together with chemical and microparticle concentrations are used to assess the signal preservation and propose a preliminary firn chronology. Airmass back trajectory analysis is incorporated to identify moisture, aerosol, and particle primary source regions and support proposed chemical and microparticle temporal variability. Short automatic weather station (AWS) records are incorporated to validate the use of the

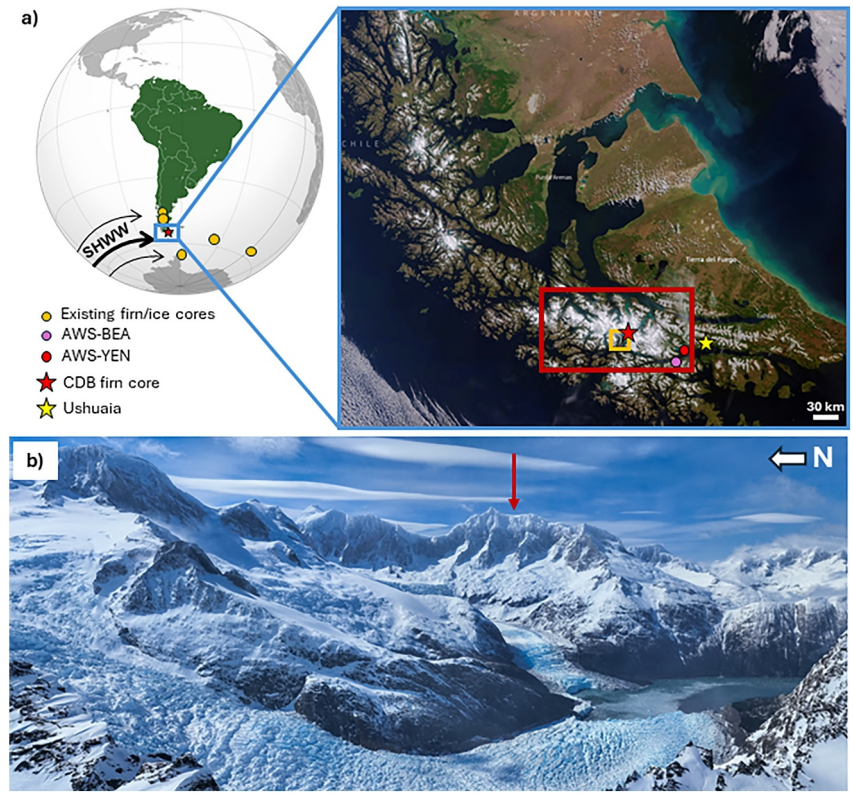

Figure 1. The Cordillera Darwin—Cresta Blanca (CDB) firn core site. (a) Map of South America with an inset of Tierra del Fuego (blue rectangle). The location of the Cordillera Darwin Icefield (red rectangle) is highlighted in relation to existing firn/ice cores and the Southern Hemisphere westerly winds (SHWWs) (SHWW). The inset presents a satellite image of Tierra del Fuego (Credit: European Union, Copernicus Sentinel-3 imagery), highlighting the location of the CDB firn core (red star) in relation to AWS sites included in this study (purple and red dots). (b) Monte Cresta Blanca from sea level to summit in October 2023 (copyright: Cristian Donoso & Cristóbal Clement). The arrow in panel (b) indicates the drilling site location. The yellow rectangle in panel (a) represents the area photographed in panel (b). Figure S1 in Supporting Information S1 presents large scale maps for the areas from where point data were extracted.

fifth generation of the European Center for Medium-Range Weather Forecasts (ECMWF) ERA5 reanalysis data for CDI and estimate local meteorological and melt conditions at different elevations. We use this information to investigate the potential of CDI to preserve valuable temporally high-resolution records from the current core of the SHWW belt.

2. Methods

2.1. Ice Core Site

In March 2020, the CODICES project drilled a 3.25 m (9 cm diameter) firn core using a Kovacs Mark II hand auger in the CDI, Chile. The drilling site was located in a flat, NW-SE oriented 150 × 150 m saddle (54.6814°S, 69.6394°W, 2324 m a.s.l), SW from Monte Cresta Blanca's summit (Figure 1), one of the highest summits in the Cordillera Darwin range. The drilling site was selected based on its high elevation (likely preventing seasonal melt), favorable flat surface for helicopter landing and ice thickness (>60 m, estimated from exposed ice cliffs). The Cordillera Darwin—Cresta Blanca firn core (CDB) drilling was stopped prematurely at 3.25 m depth due to unexpected weather conditions risking helicopter transport safety.

2.2. Sample Preparation and Analyses

2.2.1. Sample Transport and Storage

Firn core sections of 0.4–0.92 m were retrieved in the field, handled using polyethylene gloves over a pre-cleaned polyethylene surface, sealed in polythene bags, and packed in insulating boxes. The firn cores were transported

frozen (−20°C) to the British Antarctic Survey (BAS), Cambridge UK, where the cores were stored at −25°C. All the cold laboratory working surfaces were pre-cleaned using Isopropyl Alcohol (IPA). Once unpacked, firn samples were handled using polyethylene gloves over the pre-cleaned surfaces to avoid any potential contamination from the lab environment. Firn core sections were analyzed for their physical properties in the cold lab facilities at BAS. After conducting physical property measurements, firn core sections were sampled for various discrete and continuous analyses using a stainless-steel bandsaw.

2.2.2. Physical Properties

The length, diameter, and weight of each firn section was measured to obtain a density-depth profile. Firn core sections were inspected against backlight for the presence of melt layers. All visible, near-horizontal, irregular or discontinuous, bands of ice within the firn matrix, thicker than 0.5 cm, were logged, measured, and cataloged as melt layers (Orsi et al., 2015). The thickness threshold was based on Orsi et al. (2015) observation of 0.5 cm thick hard surface ("crusts") formation at WAIS Divide, likely caused by wind action.

2.2.3. Continuous Samples

Insoluble microparticle concentration (MPC) was measured using a flow-through Klotz Abakus laser particle counter connected to the BAS Continuous Flow Analysis (CFA) system (Grieman et al., 2022). Insoluble microparticles were measured in the 0.9–50 μm size range. The MPC record does not cover the full length of the core due to problems in the data acquisition and instrument saturation, particularly from 2.75 to 3.25 m. MPC spikes related to firn core breaks were removed from the MPC data set. MPC was used as the primary indicator for annual layer counting based on insoluble dust being less prone to elution during meltwater percolation (Koerner, 1997; Moser et al., 2024). Seasonal mineral dust emissions have been well-documented from Tierra del Fuego semi-arid grasslands, with their peak occurring during austral summer (Cosentino et al., 2020, 2021), thus, useful as a seasonal time marker.

Electric conductivity (EC) measurements represent the total soluble impurity content of firn (Stillman et al., 2013). EC measurements were incorporated to complement MPC measurements for annual layer counting and fill in the MPC gaps at the bottom of the record. EC was analyzed using an Amber Science flow-through meter connected to BAS CFA system.

2.2.4. Microscopy

Microscopic analyses of insoluble microparticles were included to explore the diversity, abundance, and temporal variability of pollen grains, spores, and diatoms preserved in the CDB firn core. Discrete 8 cm^2 firn sections were cut at 15 cm depth resolution for microscopic analyses. Firn samples were melted and then filtered through 13 mm diameter, 1.0 μm pore size Whatman™ Polycarbonate membrane filters, inside pre-cleaned polypropylene Swinnnex™ filter holders. Each filter was then mounted onto an aluminum stub to be analyzed on a Quanta-650F scanning electron microscope (SEM) at the Earth Sciences Department of the University of Cambridge. Each filter was imaged at 800× magnification using backscattered electron imagery (BSEI) in a low-pressure mode for microparticle identification and physical characterization, following the analysis strategy presented in Tetzner et al. (2021).

Diatom identification and ecological associations were based principally on Hasle and Syvertsen (1997), Krammer (2000) and Rumrich et al. (2000). Diatoms were identified to species level where possible. Insufficient image resolution sometimes prevented the recognition of diatom diagnostic features. In these cases, diatoms were combined in genera/morphological groups. Diatoms identified as *Fragilariopsis cylindrus* may also include F. nana (distinguished from F. cylindrus by size as per Cefarelli et al., 2010). Diatoms that were not possible to classify (e.g., fragments with undiagnostic features, and poorly ornamented or indistinct fragments) were not considered for ecological associations and assemblage composition studies but were considered in the reported total diatom count. The main diatom assemblage composition was determined from the identified species and groups with abundances higher than 2.0% of the whole assemblage. Ecological associations were determined for the species that integrated the main diatom assemblage.

The identification of pollen grains and spores was supported by a pollen reference collection and supplemented by microphotographs (Heusser, 1971; Moore et al., 1991; Shumilovskikh & van Geel, 2020; Wingenroth &

Table 1
Summary of AWS and ERA5 Grid Point Geographical Locations and Main Features of the Temperature Data Sets Analyzed in This Study

Station name	Data interval used (from-to)	Long (°W)	Lat (°S)	Elevation (m a.s.l.)	Temporal resolution	Distance to drill site (km)	Distance to nearest ERA5 grid point (km)
AWS-YEN	01/11/16–05/06/20	68.68	54.88	10	Daily	65	14
AWS-BEA	24/5/19–1/5/2023	68.7	54.95	10	30-min	66	6
ERA5-YEN/BEA	1/11/2016–1/5/2023	68.75	55	315	Hourly	66	0
ERA5-DRILL (ERA5-2000)	1/1/1979–31/12/2022	69.75	54.75	671	Hourly	12	0
DOWN-DRILL	1/1/2000–31/12/2022	69.64	54.68	2195	Daily	0.1	12
DOWN-2000	1/1/2000–31/12/2022	69.63	54.68	2018	Daily	0.6	12

Heusser, 1984). Pollen from the deciduous species *Nothofagus pumilio* and *N. antarctica*, and the evergreen species *N. betuloides* present in the region, are reported as *Nothofagus dombeyi* type, given the similarities in pollen morphology and hence difficulty in species separation.

2.2.5. Discrete Samples

Discrete firn core samples were cut at 2.5 cm resolution for stable water isotope and major ion analyses.

Ion chromatography was performed using a high-performance reagent-free Dionex Integrion ICS-2500 anion and IC 2000 cation systems in the BAS class-100 clean room. Major ions [Na^+, Ca^{2+}, NH_4^+, SO_4^{2-}, Cl^-, NO_3^-] were measured, with an average analytical precision of 0.03–0.07 ppb, to assess the seasonal preservation of soluble ions in the firn. To calculate the ionic contribution from terrestrial sources, [Na^+] and [Ca^{2+}] were used to calculate the non-sea-salt fraction of calcium [nssCa^{2+}] using the expression [nssCa^{2+}] = [Ca^{2+}]−[Na^+]* $R_{sea\ water\ Ca/Na}$ where $R_{sea\ water\ Ca/Na}$ is the mean ratio (weight by weight w/w) of Ca/Na in bulk seawater (0.038) (Bowen, 1979).

Stable water isotopes ($\delta^{18}O$ and δD) were measured using a Picarro L2130-i analyzer, with an accuracy of 0.3 and 0.9‰ for $\delta^{18}O$ and δD, respectively. Isotopic values are reported relative to the Vienna Standard Mean Ocean Water standard. Stable water isotopes were included to assess the indirect preservation of the seasonal temperature variability and potential disruptions caused by melt (Huber et al., 2024; Moser et al., 2024). The second-order isotope parameter, deuterium excess (d-excess = δD-8*$\delta^{18}O$), was calculated to explore seasonal changes in the vapor source conditions (Dansgaard, 1964; Pfahl & Sodemann, 2014).

2.3. Meteorological Data

Meteorological data are included to study the occurrence of above-freezing temperatures at high-elevation sites (≥2,000 m a.s.l.) in the Cordillera Darwin region. In situ meteorological data in this region are scarce. The nearest meteorological station, Timbales, operated by the Chilean Army, is situated 47 km southwest of the drilling site, in the fjords adjacent to the Cordillera Darwin. However, the intermittent nature of its data restricts its direct use for studying temperature variability in the region. The nearest permanently operated meteorological station is located 90 km from the drilling site, in Ushuaia, Argentina. Nevertheless, this station is situated outside the Cordillera Darwin region. Two Automatic Weather Stations (AWS), 7 km apart, provide the only continuous in situ meteorological measurements available for the Cordillera Darwin region (Table 1; Figure 1). These two stations are installed at sea level and over 60 km east from the drilling site, thus, restricting their direct use to estimate temperatures at high elevations. Climate reanalysis data offer the possibility to obtain meteorological data closer to the drilling site. However, climate reanalysis data sets must first be assessed against independent direct measurements to validate their regional use.

The two AWS data sets are used in this study to validate climate reanalysis temperature data sets. The AWS-YEN temperature data set was obtained from CR2-Explorador Climático (https://explorador.cr2.cl/) (data downloaded on the 21/11/2023). The AWS-BEA temperature data set was obtained from STARM Oceanographic Data portal (www.starm.cl) (data downloaded on the 21/11/2023). Daily AWS data sets were compared during their overlapping period (24/5/2019-5/6/2020) to cross-compare AWS measurements and assess their accuracy.

Surface air temperature data from ERA5 (Hersbach et al., 2020), was used to obtain meteorological data from the vicinity of the drilling site. Surface air temperature data sets from two ERA5 grid points (0.25° resolution) were incorporated in this study: ERA5-YEN/BEA and ERA5-DRILL (Table 1). ERA5-YEN/BEA and ERA5-DRILL grid points were selected because they are the closest ERA5 grid points to the AWS stations and the drilling site, respectively (Figure S1 in Supporting Information S1). The daily ERA5-YEN/BEA data set was compared with daily AWS data sets to assess ERA5 performance in the Cordillera Darwin region. All AWS data sets presented in this study were not previously assimilated into the ERA5 ECMWF model.

All ERA5 temperature data sets were corrected for elevation using seasonal lapse rates measured in Ushuaia's meteorological station, the only radiosonde measurements available in the vicinity of CDI. A 5.7°C/km lapse rate was used between October and March while a 7.1°C/km lapse rate was used between April and September (Buttstadt et al., 2009; Schneider et al., 2003). After correcting for elevation, ERA5 records were corrected for temperature biases obtained from the mean residuals between ERA5-YEN/BEA and AWS-BEA, and between ERA5-YEN/BEA and AWS-YEN temperature data sets. ERA5-DRILL temperature data sets were corrected for elevation and for ERA5 temperature biases, aiming to obtain the closest analogs to meteorological conditions present at the firn core site over the satellite-era (1979–2022 CE).

2.4. Downscaling Approach

A downscaling scheme (DOWN) combining statistical downscaling with radiation and orographic precipitation modeling was applied to ERA5 atmospheric parameters to produce high spatial resolution (200 × 200 m grid cell) climate variables for the CDB site (DOWN-DRILL) (Figure S1 in Supporting Information S1). The use of this downscaling routine to generate high spatial resolution climate variables has been thoroughly implemented and validated in the Cordillera Darwin Region (Temme et al., 2023). Data used in this study were generated with the same inputs as detailed in Temme et al. (2023). All DOWN temperature data sets were estimated and corrected using an annual standard moist adiabatic lapse rate (6.0°C/km) (Farnsworth et al., 2021).

Surface air temperatures were also evaluated at DOWN-2000 coordinates and at ERA5-DRILL coordinates, but at 2,000 m a.s.l. (ERA5-2000) (Figure S1 in Supporting Information S1). DOWN-2000 and ERA5-2000 were incorporated to study surface air temperature at 2,000 m of elevation and explore the potential altitude threshold for the ideal preservation of ice core records.

A Precipitation-Weighted Temperature parameter (PWT) was calculated to estimate the annual surface air temperature amplitude during precipitation events, likely related with CDB's stable water isotope annual amplitude (Brönnimann et al., 2013). The PWT parameter was calculated using DOWN-DRILL daily snowfall and surface air temperature. A minimum snowfall threshold of 1 cm was set for the PWT calculation. This threshold was set based on previous studies analyzing Antarctic snowfall reanalysis representation limitations and reported ERA5 errors in extratropical regions (Lavers et al., 2022; Tetzner et al., 2019; Thomas & Bracegirdle, 2009). A similar approach was applied to estimate snow accumulation at the CDB site. DOWN-DRILL daily snow accumulation values presented a log-normal distribution, with 79% of the days reporting precipitation below daily observed Alpine snow redistribution values (2.86 cm/day) for wind speeds between 5 and 10 m s^{-1} (Voordendag et al., 2024). Annual DOWN-DRILL snow accumulation values were estimated after accounting for potential snow redistribution in order to ensure comparability. The annual positive degree-day sum (PDD) parameter was calculated for DOWN-DRILL, DOWN-2000, ERA5-DRILL, and ERA5-2000. This parameter represents the sum of daily mean air temperatures above the melting point (0°C) during a year (Cogley et al., 2010). The annual positive degree-day sum parameter was included in this study to quantify the exposure of these sites to surface air temperatures above the melting point. A potential source of error for PDD estimated values is the use of standard or seasonal lapse rate values to correct for elevation. In absence of long radiosonde observations near CDI, the reference values used in this study (5.7 and 7.1°C/km) are the most representative estimates for the region. However, it remains unclear how representative these lapse rate values are on a daily basis and how they could contribute to increase PDD and temperature estimates uncertainty. PDD estimates, together with a reference snow degree-day factor previously used in the Southern Patagonian Icefield (4.92 ± 1.54 mm w.eq. $°C^{-1}$ d^{-1}) (Bown et al., 2019), were used to estimate annual melt production at CDB and at 2000 m of elevation. This Southern Patagonian Icefield reference value was applied to CDI because of its similar magnitude to uncertain values reported for Tierra del Fuego (4.4–4.7 mm w.eq. $°C^{-1}$ d^{-1}; Buttstädt et al., 2009). Annual PDD-derived melt estimates were compared with annual melt layer thickness in the CDB firn core to

assess accuracy of the estimate. The 10 cm w.eq. melt, roughly equivalent to ~20–30 cm of snow, was set as a threshold for the correct preservation of seasonal records in the firn, given that this amount of melt could considerably disrupt a 1-m annual firn layer (Moser et al., 2021).

A regional study of the climatological annual cycle was conducted to explore how the seasonality of some meteorological parameters could have potentially driven the variability of the records preserved in the CDB firn. Monthly reanalysis 10 m wind speed, 850 hPa relative humidity, and precipitation data sets from ERA5 were used to obtain the climatological annual cycle for an extended region centered in CDI (53–55.5°S; 67–74°W) between 1979 and 2023 CE (representative of satellite era) and between 2017 and 2019 CE (representative of CDB's top three years). The same annual cycle analysis was conducted for the surface air temperature parameter, but with a local approach (vicinities of the drill site), using ERA5-DRILL and DOWN-DRILL data. Temperature values obtained from reanalysis (ERA5) or downscaling (DOWN) are presented next to their respective root-mean-square error (RMSE) values. Common temperature statistics derived from ERA5 data set or from the down-scaled data set (DOWN) are presented next to their respective calculated Standard Deviation (SD) and Standard Error (SE) values.

2.5. Firn Core Snow Accumulation Estimation

Annual snow accumulation is derived from the annual layer thickness obtained from the CDB ice chronology. The annual layer thickness is converted to water equivalent (w.eq.) using the density-depth profile (see Section 2.2.2). Firn thinning due to vertical compaction was corrected using a Nye model (Nye, 1963).

2.6. Backward Trajectories

Back trajectory analysis is performed to track the transport pathways followed by air masses before reaching the Cordillera Darwin. Three-dimensional air parcel pathways were calculated using the National Oceanic and Atmospheric Administration's Hybrid Single-Particle Lagrangian Integrated Trajectory model (NOAA—HYSPLIT) (Draxler & Hess, 1998; Stein et al., 2015). Back trajectories were initiated from the CDB drilling site (2,324 m a.s.l.) at mid-day, every day, between the 1st of October 2016 and the 6th of March 2020. This period was selected because it covers the proposed CDB chronology (see Section 3.3). Each trajectory was calculated over a 120-hr (5 days), 24-hr, and 6-hr period, using the NCEP/NCAR Reanalysis archives (1948–present) (2.5° latitude-longitude resolution). These periods were selected to ensure the trajectories represented the transport of small and large particles, from their source, until reaching CDB. Back trajectories are presented as annual and seasonal compilations. For each compilation, a back trajectory cluster analysis was generated incorporating all the trajectories during the correspondent time interval. Back trajectory clusters were calculated using the HYSPLIT clustering tool. The optimal number of clusters to be calculated was decided based on the "elbow method" which allows identifying the minimum number of clusters to calculate while representing the maximum variance. Each cluster plot shows the most frequent trajectories followed by air masses and the percentage of trajectories, among all trajectories, that were incorporated into each cluster path. Back trajectory frequency plots show the sum of the number of trajectories that passed through each grid cell divided by the total number of trajectories analyzed.

3. Results

3.1. Meteorology

3.1.1. Evaluating the Representativity of ERA5 Temperature Estimates

During their overlapping period (24/5/2019-5/6/2020), ERA5-YEN/BEA, AWS-BEA, and AWS-YEN show similar daily mean surface air temperature values (+5.85°C, +6.29°C and +6.53°C, respectively), with ERA5 presenting a cold bias of −0.52°C (SD: ±1.17°C; SE: 0.06°C) (Figure S2 in Supporting Information S1). There is a statistically significant positive correlation between the daily mean surface air temperature values from both AWS stations ($R = 0.97$, $p < 0.01$, $n = 373$). Similarly, there is a statistically significant positive correlation between the daily mean surface air temperature values of ERA5-YEN/BEA and AWS-BEA ($R = 0.96$, $p < 0.01$, $n = 379$), and of ERA5-YEN/BEA and AWS-YEN ($R = 0.94$, $p < 0.01$, $n = 373$).

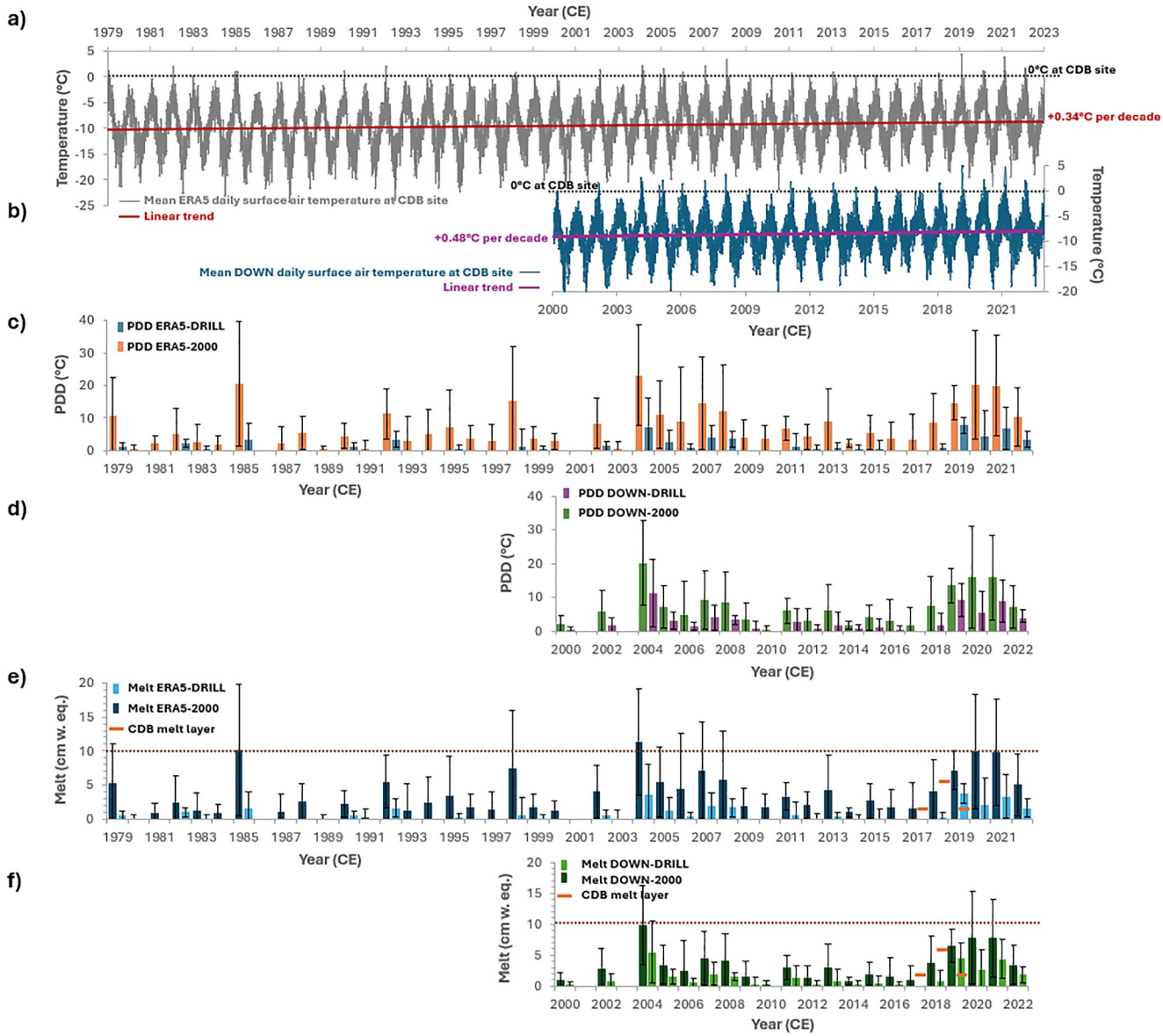

Figure 2. Estimated temperature and melt timeseries in the vicinity of the CDB drilling site. (a) ERA5-DRILL daily mean surface air temperature timeseries (1979–2022 CE). Red line indicates the linear trend. (b) DOWN-DRILL daily mean surface air temperature timeseries (2000–2022 CE). Purple line indicates the linear trend. (c) PDD timeseries for ERA5-DRILL (blue) and ERA5-2000 (orange). (d) PDD timeseries for DOWN-DRILL (purple) and DOWN-2000 (green). (e) Estimated melt timeseries for ERA5-DRILL (light blue) and ERA5-2000 (dark blue). (f) Estimated melt for DOWN-DRILL (light green) and DOWN-2000 (dark green). Black lines in panels (c–f) represent error bars. Orange line in panels (e, f) represent observed total annual melt layer thickness at CDB site. Brown dashed lines in panels (e–f) represent the 10 (cm w.eq.) threshold.

3.1.2. Surface Air Temperatures in the CDB Area

Daily mean surface air temperature in the vicinity of the CDB drilling site (ERA5-DRILL) is estimated to be −9.39°C (SD: ±3.94°C; SE: 0.03°C) (1979–2022 CE) with a positive trend of +0.34°C per decade (Figure 2a). Similarly, the daily mean surface air temperature at DOWN-DRILL over the downscaling evaluation period (2000–2022 CE) is estimated to be −8.51°C (SD: ±3.38°C; SE: 0.04°C) with a positive trend of +0.48°C per decade (Figure 2b).

The climatological (1979–2022 CE) surface air temperature annual cycle indicated by ERA5-DRILL shows the highest annual temperatures occur during February and the lowest temperatures during July (Figure S3 in Supporting Information S1), with a mean annual amplitude of 9.83°C (SD: ±1.42°C; SE: 0.21°C). When evaluated

over 2017–2019 CE, representative of CDB's top three years, the annual cycle is slightly shifted, presenting the lowest temperature during June at ERA5-DRILL and at DOWN-DRILL. For the 2017–2019 CE period, DOWN-DRILL surface air temperature estimates, with a comparatively higher spatial resolution, indicate a mean annual amplitude of 8.15°C (SD: ±1.12°C; SE: 0.65°C) and a PWT mean annual amplitude of 7.64°C (SD: ±1.84°C; SE: 1.06°C) (Figure S4 in Supporting Information S1).

Over the ERA5 evaluation period (1979–2022 CE), ERA5-DRILL presented 57 days (out of 16,071) of daily mean surface air temperatures above the freezing point, with a mean value of +1.01°C (SD: ±0.98°C; SE: 0.13°C) and an absolute maximum of +4.33°C (RMSE: 1.29°C) on 5/2/2019. Of these days, 72% occurred after the year 2000 CE. The PDD parameter for ERA5-DRILL presented a mean value of +1.31°C (SD: ±2.05°C; SE: 0.31°C), with an absolute maximum of +7.67°C (SD: ±2.82°C; SE: 0.10°C) (2019 CE) and a considerable increase in PDD frequency and magnitude since 2004 CE (Figure 2c). A mean annual melting of 0.64 cm w.eq. (SD: ±1.01 cm w.eq.; SE: 0.15 cm w.eq.) was estimated for ERA5-DRILL, with a maximum of 3.77 ± 1.4 cm w.eq. in 2019 CE (Figure 2e).

Over the downscaling evaluation period (2000–2022 CE), the DOWN-DRILL site presented 50 days (out of 8401) of daily mean surface air temperatures above 0°C, with a mean value of +1.22°C (SD: ±1.13°C; SE: 0.16°C) and an absolute maximum of +4.87°C (RMSE: 1.25°C) occurring on 5/2/2019. The PDD parameter for DOWN-DRILL presented a mean value of +2.65°C (SD: ±3.20°C; SE: 0.67°C), with an absolute maximum of +11.14°C (RMSE: 1.25°C) during the austral summer 2003/2004 CE (Figure 2d). DOWN-DRILL exhibited a mean annual melting value of 1.31 cm w.eq. (SD: ±1.58 cm w.eq.; SE: 0.33 cm w.eq.), with a maximum of 5.48 ± 4.99 cm w.eq. in 2004 CE (Figure 2f).

ERA5 daily mean surface air temperature in the vicinity of the CDB site, at 2000 m of elevation (ERA5-2000), is estimated to be −7.31°C (SD: ±3.77°C; SE: 0.03°C). Since 1979, 247 days presented above-zero temperatures. During these 247 days, daily mean surface air temperatures was +1.23°C (SD: ±1.11°C; SE: 0.07°C), with an absolute maximum of +6.17°C (RMSE: 1.29°C). The PDD parameter for ERA5-2000 presented a mean value of +6.89°C (SD: ±6.27°C; SE: 0.92°C) between 1979 and 2022, with a maximum of +23.11°C (RMSE: 1.29°C) in 2004 (CE) and higher-than-average values concentrated over the last two decades (Figure 2c). The ERA5-2000 melt estimation presented a mean annual value of 3.39 cm w.eq. (SD: ±3.01 cm w.eq.; SE: 0.45 cm w.eq.), with a maximum of 11.37 ± 7.81 cm w.eq. in 2004 CE.

DOWN-2000 daily mean surface air temperature (2000–2022 CE) is estimated to be −7.44°C (SD: ±3.38°C; SE: 0.04°C). Over the downscaling evaluation period, 114 days presented daily mean surface air temperatures above 0°C. The mean surface air temperature during these days was +1.31°C (SD: ±1.17°C; SE: 0.11°C), with a maximum of +5.94°C (RMSE: 1.25°C). The PDD parameter for DOWN-2000 presented a mean value of +6.40°C (SD: ±5.44°C; SE: 1.13°C), with an absolute maximum of +20.12°C (RMSE: 1.25°C) in austral summer 2004 (CE) (Figure 2d). The DOWN-2000 data set presented a mean annual melting value of 3.15 cm w.eq. (SD: ±2.68 cm w.eq.; SE: 0.56 cm w.eq.), with a maximum of 9.90 ± 6.34 cm w.eq. in 2004 CE (Figure 2f).

Data presented in Section 3.1.2 is summarized (Table S1).

3.1.3. Regional Climatological Annual Cycle

The regional climatological (1979–2023 CE) wind speed annual cycle shows stronger-than-average winds during austral spring-summer (Figure S3 in Supporting Information S1). Over the targeted period (2017-19 CE), stronger-than-average winds occur during austral spring-summer, with this summer winds being considerably stronger than the climatological summer wind. The relative humidity annual cycle, for the climatological and targeted period, presents minor variability throughout the year (74%–82%), with the highest values during austral summer and the lowest values during austral winter. The regional climatological precipitation annual cycle exhibits higher-than-average values between austral mid-spring and early autumn, when precipitation is ∼50% higher than during austral winter. The annual cycle of precipitation over the targeted period follows a similar pattern to the climatological annual cycle, but with considerably (∼25%) higher precipitation during December-January.

3.1.4. Downscaled Snow Accumulation Estimation at the CDB Site

The DOWN-DRILL snowfall data set (accounting for snowdrift) revealed a total of 80, 84, and 70 snowfall days (≥2.86 cm/day) for the years 2017, 2018 and 2019, respectively. The annual snow accumulation at the CDB site is estimated to be 0.59, 0.62, and 0.48 m w.eq. for years 2017, 2018, and 2019, respectively, when using the CDB density-depth profile (See Section 3.2.1).

3.2. Firn Analyses

3.2.1. Firn Physical Properties

The CDB density-depth profile describes a logarithmic growth, with values increasing from 450 (kg/m^3) at the surface to ~600 (kg/m^3) at the bottom of the core. Visual logging of the CDB firn core enabled the identification of a wide variety of thin (<1–2 mm) ice features and wind crusts intercalated within the firn. Seven melt layers >0.5 cm were evident, with thickness ranging up to 5 cm (Figure 3).

3.2.2. Major Ions

[Na^+], [Cl^-], and [SO_4^{2-}] were the largest contributors to the CDB ion budget, with mean concentrations of 406, 249, and 104 ppb, respectively. Together, they account for 86% of CDB total ion concentration. The mean CDB [Cl^-]:[Na^+] ratio was 1.67. The ion concentration-depth profiles of these three species presented similar variability, drawing three clear periodic cycles down-core. Higher concentrations were centered at 0.15, 1.05, 2.30, and 2.97 m (Figure 3b).

The other ions, [nssCa^{2+}], [NO_3^-], and [NH_4^+], are comparatively less concentrated, with mean values of 54, 36, and 7.6 ppb, respectively. [nssCa^{2+}] and [NO_3^-] presented similar cyclicity to the most concentrated ions, with the exception of an absent enhancement in [nssCa^{2+}] at ~2.3 m (Figure 3d). In turn, [NH_4^+] presents a higher-frequency variability, when compared with [nssCa^{2+}] and [NO_3^-], with less clear cyclicity. Nevertheless, [NH_4^+] peaks were still identifiable and align with previously identified cation and anion enriched horizons (Figure 3c).

3.2.3. Stable Water Isotopes

$\delta^{18}O$ values ranged between −7.4‰ and −17‰, with a mean value of −13.1‰ (±1.9‰). δD values ranged between −49.9‰ and −129.7‰, with a mean value of −97.6‰ (±15.5‰) (Figure 3e). Both isotope-depth profiles exhibit a negative trend (−11.3 (‰/m) for δD) with the lowest values at the bottom of the core. CDB stable water isotope depth profiles exhibits low-range variations with no clear seasonality (Figure 3e). The linear $\delta^{18}O$–δD relationship was used to obtain a Local Meteoric Water Line (LMWL) for the Cordillera Darwin, $\delta D = 8.12*\delta^{18}O + 9.07$ ($R^2 = 0.99$, $p < 0.01$).

Mean deuterium excess (d-excess) was 7.4‰ (±1.2‰) with values ranging from 5.3 to 11‰ (Figure 3e). The CDB d-excess record is characterized by 2 cycles of higher-than-average values (centered around 1.2 and 2.15 m) followed by intervals of lower-than-average values (between 1.3–1.8 m and 2.4–2.7 m). Above 1.20 m and below 2.7 m, this cyclicity is less conspicuous and obscured by higher and lower amplitude variability, respectively.

3.2.4. Insoluble Microparticles

Microparticle concentrations (MPC) values ranged from 11,400 (particles/ml) to 600 (particles/ml), with a mean value of 2,500 (particles/ml) (Figure 3a). The MPC-depth profile is characterized by 2.5 cycles of higher-than-average values (centered around 1.02 and 2 m, when values consistently exceed 4,000 particles/ml) followed by intervals of lower-than-average values (with lowest values between 0.3 and 0.5 m, 1.4–1.5 m, and 2.4–2.5 m).

The most abundant microparticles observed were assortments of amorphous mineral dust grains, diatoms, pollen grains, and spores. A total of 660 diatom valves and fragments were found in the CDB firn core. Diatoms were well preserved with many intact cells (two valves and a girdle band) and colonies of up to four cells. There is no statistically significant correlation between the diatom abundance and the volume of meltwater filtered per sample ($R = 0.03$, $p > 0.05$ $n = 21$). The total diatom concentration presented a mean value of 429 (diatoms L^{-1}). The total diatom concentration-depth profile exhibits three cycles, with diatom enhancements at 0.15, 1.20, 2.25, and 3 m (Figure 3f). Of the total diatoms counted, 455 (69%) were identified to genus level or higher. A total of 48

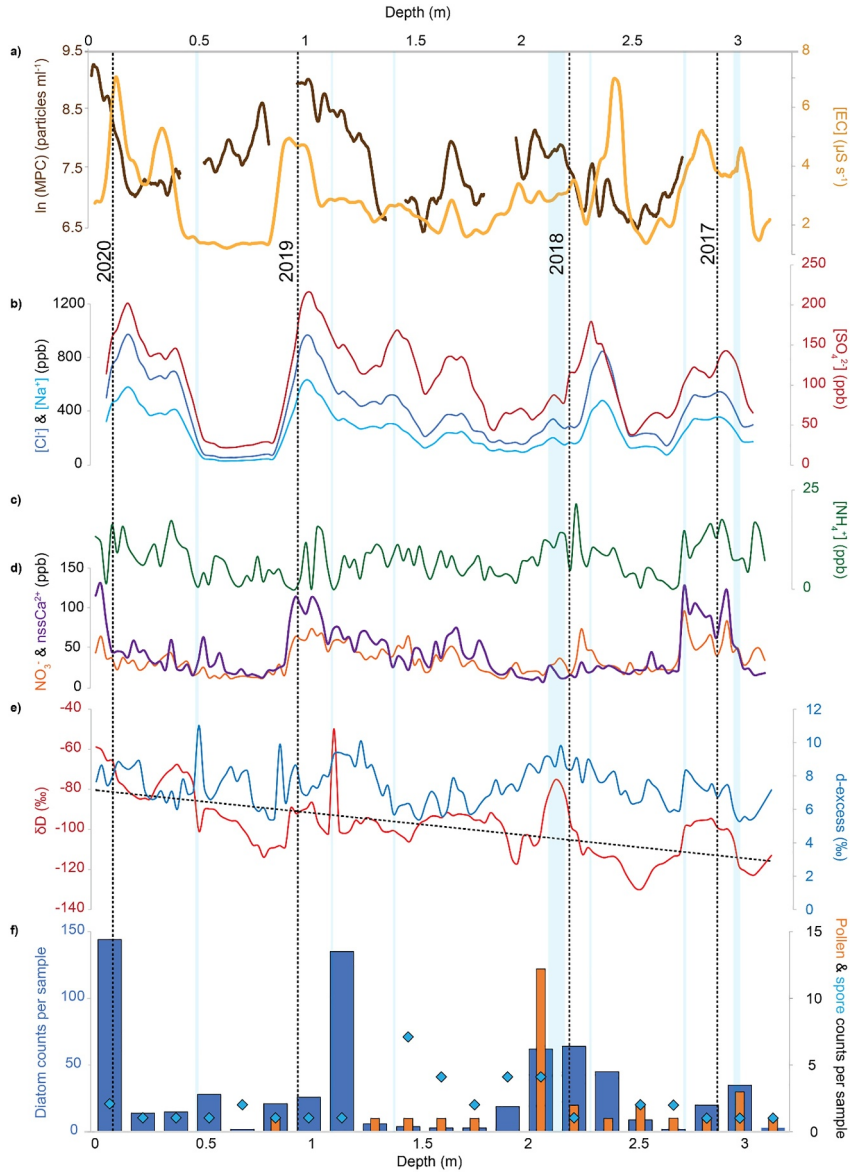

Figure 3. CDB firn core chemical and insoluble microparticle records. (a) Insoluble microparticle concentration (brown) and electric conductivity (yellow). (b) Cl^- (dark blue), Na^+ (light blue), and SO_4^{2-} (red) concentrations. (c) NH_4^+ concentration (green). (d) $nssCa^{2+}$ (purple) and NO_3^- (orange) concentrations. (e) δD (red) and d-excess (blue). (f) Diatom (blue bars), pollen (orange bars), and spore (light blue diamonds) counts per sample. Vertical pale blue lines represent the position and thickness of melt layers. Vertical black dashed lines indicate the austral early summer peak depth (January).

diatom species and genus–taxon groupings were identified. Of these, five occurred at ≥2% relative abundance, representing 63.2% of the identified diatoms.

The CDB main diatom assemblages comprised *Pinnularia* spp. (43%), *Luticola* spp. (25%), *Nitzschia* spp. (23%), *Fragilariopsis cylindrus* (6%), and *Cyclotella* s.l. group (4%). *Pinnularia* spp. was comprised of mostly *P. borealis* s.l., characteristic of subaerial environments (e.g., soils, ephemeral ponds) (Pinseel et al., 2020). *Luticola* spp. was mostly comprised of *Luticola cf. mutica/cohnii* and *Luticola cf. muticopsis*, common in sub-aerial habitats, moist soils, stream edges, among moss patches and cryoconite holes (Kociolek et al., 2017). *Nitzschia* spp. was comprised of unspecified fragments of Nitzschia sensu lato, a cosmopolitan genus with freshwater and marine species (Lowe, 2003). The *Cyclotella* group is comprised of unspecified specimens of *Cyclotella* sensu lato (including *Lindavia, Discostella, Tertiarius,* and *Pantocsekiella* and other morphologically similar types), a cosmopolitan genus complex with broad ecological affinities across aquatic environments (Lowe, 1975).

Of the five key taxa identified in the diatom assemblages, only one, *F. cylindrus*, is exclusively marine (sea-ice-affiliated diatom). The remaining four taxa have been identified in marine, freshwater, and brackish environments (Bagmet et al., 2022; Ciniglia et al., 2007; Kociolek et al., 2017; Lowe, 1975) and can be found in the Patagonia region and its surrounding ocean (Almandoz et al., 2011; Espinosa, 2008; Pinseel et al., 2020; Simonato et al., 2017). The three most abundant diatoms are almost exclusively present at the depths where total diatom enhancements were identified.

A total of 39 pollen grains were found in the CDB ice core. Pollen grains were found in various states of preservation, with 59% of the pollen grains being crumpled and 5% broken. The pollen-depth profile was characterized by a major enhancement centered at 2.1 m depth (Figure 3f). Of all the pollen grains counted, 28 (72%) were possible to identify to their family/species level. The most abundant pollen grain found was *Nothofagus dombeyi*-type (64%), common from evergreen and deciduous species in the west Patagonia region (McCulloch et al., 2022). Less abundant herbaceous pollen types found at CDB are typical of the Southern Patagonia steppe and montane flora (e.g., *Empetrum rubrum*, *Poaceae*) (Lorion & Small, 2021; Mancini et al., 2012).

A total of 44 spores were found in the CDB ice core. The spore-depth profile presents a major enhancement at 1.5 m depth (Figure 3f). Of all the spores found, 39 were identified to their family/species level. The most abundant spores were fungal Basidiospores (21%), *Gelasinospora* spp. (13%), and *Sordaria*-type (23%). Windblown fungal Basidiospores are commonly found as aerosols in the atmosphere year-round (Hassett et al., 2015). *Gelasinospora* is a genus closely related to *Sordaria*-type. While the presence of *Gelasinospora* spp. spores is commonly associated with forest-steppe ecotone communities in Tierra del Fuego, the presence of *Sordaria*-type spores is indicative of the presence of herbivorous grazers (Musotto et al., 2017).

3.3. CDB Chronology

The CDB chronology was derived using annual layer counting and assumes that the observed cyclicity in chemical and microparticles derives from seasonal deposition. Mineral dust emissions from Tierra del Fuego's semi-arid grasslands have a marked seasonality, with clear enhancements during the austral summer (Cosentino et al., 2020, 2021). The seasonal variability in mineral dust deposition has been used previously for annual layer counting in ice cores from the Andes region (Reis et al., 2022; Thompson et al., 1979), therefore, enabling its use for the CDB chronology development. The identified MPC and EC enhancements were, therefore, assigned as austral summer datums, with peaks representing approximately the early-to-mid austral summer (January/February). The ascribed chronology of the CDB core extends from approximately austral spring 2016 until late summer 2020 (Figure 3).

3.4. Snow Accumulation

Based on the CDB chronology, the mean annual snow accumulation at CDB drill site was estimated to be 0.51 m w.eq. for the period between January 2017 and January 2020. Snow accumulation estimates were 0.5, 0.57, and 0.45 m w.eq. for the years 2017, 2018, and 2019, respectively.

3.5. Melt Estimation Assessment

Based on the CDB chronology, the total annual melt layer thickness (see Section 3.2.1) magnitude is similar ($\leq$5.5 cm w.eq.) to total annual melt estimated at CDB drill site using ERA5 and DOWN data sets (Figures 2e and 2f), with melt layer thickness being comparatively higher on 2017 and 2018, and lower on 2019.

3.6. Back Trajectory

Back trajectory analyses show >90% of all air masses reaching CDB originate from the southeastern Pacific Ocean and the Amundsen and Bellingshausen Seas (Figure 4), and travel over the 50°–60° latitudinal band with slight variations throughout the year (Figures S5 and S6 in Supporting Information S1). Austral autumn-winters (April to September) present a slight increase (~5–10%) in the number of trajectories originating south of the 60°S latitudinal band. In turn, austral spring-summer (October to March) present a slight increase (~5–10%) in the number of trajectories originating north of the 50°S latitudinal band. Given CDI's location, all trajectories have a short interaction with land before reaching CDB (Figures 4b and 4c). The trajectory frequency analysis show that

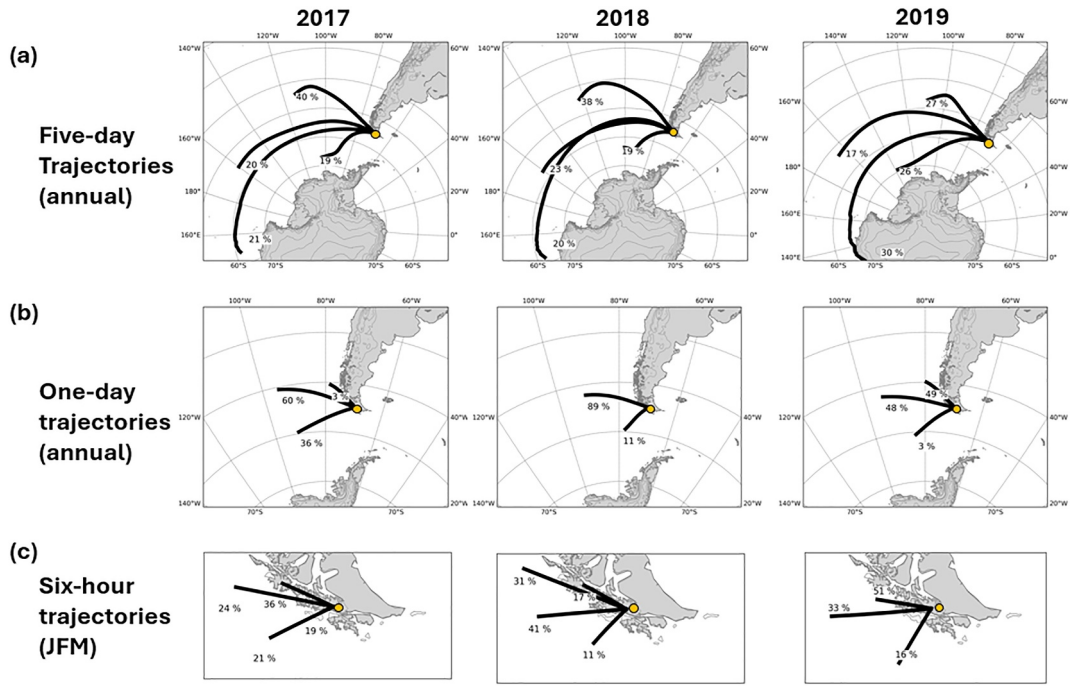

Figure 4. Maps of Antarctica, the Southern Ocean, and South America showing the clusters of all 5-day, 1-day, and 6-hr air mass trajectories reaching the CDB site throughout the year. The yellow circle indicates the location of the CDB site. Percentages indicate the relevance of each cluster.

~80–90% of all the trajectories (2016–2020 CE) traveled over the Chilean fjords, northwest of CDB (Figure S7 in Supporting Information S1).

4. Discussion

4.1. Chemical and Microparticle Record Preservation

Annual positive degree-day sum (PDD) estimates for ERA5-DRILL and DOWN-DRILL, obtained from validated and corrected ERA5 mean daily temperatures, suggest the CDB site had been progressively exposed to temperatures above the freezing point (Figure 2). This trend has indicated the potential to produce surface melt which may disrupt the chemical and microparticle records preserved in the CDB firn (Moser et al., 2024). Disruptions to the firn matrix caused by melt and percolation are characterized by the abnormal densification of the firn, visible as melt features and the homogenization or attenuation of chemical species down-core in the affected section (Moser et al., 2024). Our physical firn properties reveal a normal logarithmic densification pattern for the CDB firn core, with only few, thin, and limited melt layers. Observed melt layers were not directly aligned with chemical or microparticle peaks, therefore, suggesting that ion concentration and microparticle increases were not caused by melt alteration. Despite PDD values suggesting that CDB could have been progressively exposed to temperatures above freezing, firn core melt layer observations confirm that shallow firn layers at this site have not been substantially disrupted by melt. These observations are further supported by melt estimates suggesting snow melt has been limited at the CDB drill site over the satellite-era, with annual melt values permanently below 10 (cm w.eq.). Although melt estimates and melt layer thickness observations broadly agree on their magnitude, they presented considerable discrepancies in their variability (Figure 2). These discrepancies could indicate that the use of Ushuaia's summer seasonal mean lapse rate over daily/synoptic timescales (5.7°C/km; ERA5-DRILL) or a constant standard moist adiabatic lapse rate (6.0°C/km; DOWN-DRILL), has led to small overestimations of CDB summer surface air temperatures and, consequently, PDD and melt values at CDB. The high relative humidity of air parcels reaching CDI during the austral summer (RH > 80%) (Figure S3c in Supporting Information S1) supports a slightly more saturated adiabatic lapse rate which should be more realistic for summer conditions in this region (4.5–5.5°C/km), as reported in the sub-Antarctic Marion Island (47°S) (Hedding, 2006). The preservation of undisrupted firn at this elevation is supported by previous firn

cores drilled at similar elevations from the Southern Patagonian Icefield (Aristarain & Delmas, 1993; Schwikowski et al., 2006, 2013). Our results support that CDB firn has not been significantly disrupted by melt and percolation but cannot discard significant surface melt occurring below 2,000 m a.s.l., in line with previous reports of considerable surface melt occurring at 1,800 m a.s.l. in Cordillera Darwin (February–March 2006) (Mayewski et al., 2016) and below 1,800 m a.s.l. in the Patagonian Icefields (Kohshima et al., 2002; Matsuoka & Naruse, 1999; Yamada, 1987).

Major ion profiles preserved in the undisrupted CDB firn record reveal clear and consistent variability down-core, likely indicating temporal changes in the ion load. Major ion peaks were found proximal, but not aligned, to constrained melt layers and are consistently preceding MPC and conductivity enhancements. The Patagonia region and its surrounding ocean is characterized by a marked seasonal wind regime (See Section 3.1.3), with austral spring/summer higher-than-average wind speeds in the Patagonia coast enhancing sea-spray formation (Adame et al., 2019; Carrasco et al., 2002; Grigholm et al., 2009; Ovadnevaite et al., 2012). The close similarity between the CDB $[Cl^-]$:$[Na^+]$ ratio (1.67) and the bulk sea water $[Cl^-]$:$[Na^+]$ ratio (1.8) (Hutton, 1977), indicates a predominantly marine source for these ions, implying rapid aerosol transport. A marine source is supported by back trajectories which indicate that most air parcels reaching CDB originated in the southeast Pacific Ocean and the Amundsen and Bellingshausen Seas (Figure 4). The enhanced wind-driven seasonal emission of marine aerosols along the Patagonia coast and its effective atmospheric transport supports a marked seasonal deposition of marine-sourced $[Cl^-]$ and $[Na^+]$ at the CDB site. A predominantly marine origin for these ions is consistent with previous fresh snow studies conducted in the CDI (Grigholm et al., 2009), firn cores from the Patagonian Icefields (Aristarain & Delmas, 1993; Schwikowski et al., 2006; Vimeux et al., 2008), and firn cores from the northern Antarctic Peninsula (Hoffmann-Abdi et al., 2023; Jiahong et al., 1998; Simoes et al., 2004). $[Cl^-]$ and $[Na^+]$ enhancements have been previously documented and identified as summer peaks in a core from the Southern Patagonian icefield (Schwikowski et al., 2006).

Continentally-sourced ions ($[NO_3^-]$, $[NH_4^+]$, and $[nssCa^{2+}]$) traditionally derived from biomass burning, biomass emissions, and soil erosion, also present a marked increase during austral summer in the Patagonia region (Holz & Veblen, 2011). Similarly, preferential mineral dust mobilization from erodible soils in Patagonia and Tierra del Fuego during the arid season (austral summer) promote the availability of $[nssCa^{2+}]$ (Cosentino et al., 2021). Back trajectories show most air parcels were transported over, at least 100 km of forested fjords and/or semi-arid land right before reaching the CDB site (Figure 4), likely incorporating continentally-sourced ions on their way (Gong et al., 2022). The enhanced seasonal emission of continental ions, together with its effective atmospheric transport support the seasonal deposition of these ions at the CDB site. Comparable $[nssCa^{2+}]$ summer peaks from Patagonian mineral dust sources have been previously reported in a Patagonian ice core (Vimeux et al., 2008), validating the $[nssCa^{2+}]$ seasonality as a regional feature.

The diatom record preserved in the CDB core varies down-core with large increases in abundance coincident with major ion and MPC peaks (Figure 3). Diatom identification, ecological affinities, and back trajectories indicate diatoms reaching the CDB site could have originated from the wide variety of aquatic environments present in the South Pacific Ocean and Southern Patagonia, with predominant freshwater species suggesting non-marine habitats as the primary sources (e.g., lakes, ponds, stream edges, moist soils). Diatom productivity in the South Pacific Ocean and Southern Patagonia is light-limited, with strong blooms occurring during the austral spring (Almandoz et al., 2011; Deppeler & Davidson, 2017; Flores-Melo et al., 2024). Similarly, the considerable May-to-September snow cover in Tierra del Fuego (Pitman, 2023) likely limits the uplift of locally sourced freshwater diatoms to austral spring and summer, when the climatological annual cycle supports strongest winds occur (See Section 3.1.3). This marked seasonal diatom availability enables us to use the diatom record as a biological tracer and interpret the CDB diatom peaks as austral spring markers, providing independent evidence of elevated major ion concentrations during summer at the CDB site.

The CDB chronology can further be corroborated by modelled snow accumulation estimates, and using pollen grains found at the CDB site. Annual snowdrift corrected DOWN-DRILL snow accumulation estimates' magnitude and variability (see Section 3.1.4) are in close agreement with annual firn snow accumulation estimates derived from CDB chronology (see Section 3.4), therefore, further supporting the proposed CDB chronology.

Land pollen grains and spores found at CDB can only be sourced from terrestrial environments. Back trajectories confirm the Southern Patagonian region as the only landmass interacting with the air parcels reaching the CDB

site (Figure 4), suggesting CDB pollen grains and spores are locally sourced. A local source for pollen and spores is further supported by their taxonomical classification indicating they correspond to common species found in the Patagonia region. The notable peak in the pollen grain record occurs slightly after the diatom peak, likely during the austral summer of 2018. The proposed austral summer enhancement for locally sourced pollen is consistent with pollen grain dispersal in the Southern Patagonia region, reaching its peak during austral spring-summer (Hechenleitner et al., 2005; Toro Manriquez et al., 2016). The presence of a prominent pollen peak and the absence of pollen peaks in neighboring years is consistent with previous results observed in an ice core from the Southern Patagonian icefield (Schwikowski et al., 2013). Schwikowski et al. (2013) suggested the absence of regular austral summer pollen peaks can be explained by the inter-annual variability in mast flowering. The prolific wind pollinators of *Nothofagus* are considered to be masting species (Toro-Manríquez et al., 2023) which may create apparent hiatuses in the pollen record. Complementarily, apparent hiatuses in pollen deposition may be associated with wind-scouring events during austral summer. Given that austral summer pollen peaks are not a consistent feature of the record, their use as seasonal markers is limited. Where found, however, cyclical variations in pollen concentrations can be used to confirm individual annual layers.

The stable water isotope and d-excess records at CDB show no clear seasonal variability or pattern consistent with the CDB chronology. Stable water isotopes have been traditionally used in ice core research because of their clear seasonal cycle driven by a strong linear relationship with air condensation temperature (Dansgaard, 1964). However, this is not always the case for ice cores in mid and tropical latitudes (Liu et al., 2023; Thompson et al., 1995). Near-surface post-depositional processes (e.g., melt/refreeze, diffusion, sublimation and condensation, wind drift) can dampen the stable water isotope seasonal signal (Casado et al., 2021; Moser et al., 2024), although the thin melt layers observed at CDB suggest the effects of melt and refreeze are small. The close similarity between the LMWL slope (8.12) and the GMWL slope (8.00) further supports the limited effect of melt over the CDB record. Diffusion is not considered to play an important role smoothing the CDB stable water isotope record because annual layers are considerably larger than the typical firn diffusion length (<15 cm) (Gkinis et al., 2021). Sublimation or condensation between the snow surface and near-surface air can produce isotopic exchanges in the snowpack leading to secondary fractionation (Casado et al., 2018). The summits of Cordillera Darwin are almost permanently cloud covered (Carrivik et al., 2016; Mayewski et al., 2016) and under high relative humidity conditions throughout the year (≥74% RH), therefore, favoring surface condensation which can disrupt the CDB seasonal isotopic profile.

The CDB site, located in the core of the SHWW (SHWW) belt, is also constantly exposed to strong winds likely to induce wind drift. Wind drift causes the removal and redistribution of surface snow, potentially creating stratigraphical hiatuses, hardened surfaces (wind crusts) and/or the redeposition of snow removed from other surfaces (Ekaykin et al., 2002), disrupting the stable water isotope seasonal cycle. The strong mean annual wind speed at CDI (8 m/s, Grigholm et al., 2009) lies between the threshold wind speed for the initiation of wet (9.9 m/s) and dry (7.7 m/s) blowing snow (Li & Pomeroy, 1997), suggesting recurring wind drift conditions. The wide presence of thin (<2 mm), bubble-sparse high-density crusts, probably caused by wind, within the CDB firn supports the frequent occurrence of wind ablation and wind scouring. The climatological annual cycle supports most wind scouring and ablation will occur in austral summer, in phase with the highest snow accumulation, therefore, limiting seasonal hiatuses in the record (See Section 3.1.3). In addition, the consistency in the annual layer thickness interpreted from CDB major ion and microparticle records, in line with downscaled snow accumulation estimates, does not indicate large hiatuses in the record. However, we cannot rule out the occurrence of frequent, minor wind drift events, mostly during austral summer, causing the removal, mixing, homogenization, and/or hardening of surface snow. Our results align with previous studies reporting wind drift among the main post-depositional processes disrupting Patagonia and northern Antarctic Peninsula firn core records (Aristarain & Delmas, 1993; Fernandoy et al., 2018; Hoffmann-Abdi et al., 2023; Schwikowski et al., 2006; Vimeux et al., 2008).

In addition to post-depositional processes, precipitation intermittency, regional intra-annual changes in moisture source location and condensation conditions can directly hinder the development of the stable water isotope seasonality (Casado et al., 2020; Hoffmann-Abdi et al., 2023). Precipitation intermittency may impact the development of a clear, symmetrical, stable water isotope annual cycle by producing comparatively larger snow deposition over a season. Our results demonstrate considerably higher precipitation during austral spring-summer at CDB (~50% higher than austral winter) (see Section 3.1.3), suggesting precipitation intermittency could hinder the formation of clear stable water isotope seasonality. The second-order parameter, deuterium excess, show no

marked seasonality aligned with the CDB chronology, suggesting a relatively constant moisture source for CDB. A constant moisture source region is also supported by back trajectories originating from the southeast Pacific Ocean (50–60°S) throughout the year (Figures S5 and S6 in Supporting Information S1). This moisture source is characterized by a low dew point temperature, likely promoting condensation when airmasses reach the Cordillera Darwin orographic barrier. A high condensation rate in the Cordillera Darwin region is supported by the limited amplitude in the relative humidity annual cycle (74%–82%) (see Section 3.1.3), evidencing the mountain range is permanently under high relative humidity conditions. Condensation temperature is a key parameter defining the isotopic ratios preserved in the firn record (Markle & Steig, 2022). The proximity between the moisture source and the precipitation site suggests condensation occurs under Cordillera Darwin's strong maritime climate conditions (Hall et al., 2013; Holmlund & Fuenzalida, 1995). A maritime climate is characterized by the presence of a large water body buffering seasonal temperature extremes and, therefore, reducing the amplitude of air temperature and condensation temperature over the year (Oliver, 2005). A small annual amplitude in air and condensation temperature is evidenced by CDB's annual temperature cycle analyses, showing the annual mean air temperature and annual precipitation-weighted temperature amplitudes are 8.15°C and 7.64°C, respectively (see Section 3.1.2). This small amplitude in annual condensation temperature could explain the absence of clear seasonality in the CDB stable water isotope record. A dominant local moisture source with small relative humidity variability throughout the year and a supressed stable water isotope seasonality due to the strong maritime climate at CDB is consistent with stable water isotope records obtained from other firn cores drilled in Patagonia (~600 km north of CDB) and the northern Antarctic Peninsula (~1,000 km south of CDB) (Fernandoy et al., 2018; Hoffmann-Abdi et al., 2023; Jiankang et al., 2001; Simoes et al., 2004; Schwikowski et al., 2006; Vimeux et al., 2008). Despite these numerous factors potentially explaining the lack of a clear seasonality, CDB's stable water isotope records could still hold valuable environmental data (e.g., synoptic events and moisture source variability), as seen in coastal Antarctic cores (Goursaud et al., 2019; Hoffmann-Abdi et al., 2023). However, its current interpretation is limited by the shortness of the record.

4.2. Implications and Potential for Future Ice Core Research in the Cordillera Darwin Icefield

CDB is the first firn core recovered from the 1,600 km latitudinal gap between the Southern Patagonian icefield and the northern Antarctic Peninsula. The CDB core provides the first reference for the background chemical composition and microparticle content preserved in the CDI over intra and inter-annual timescales. Furthermore, the CDB diatom, pollen, and MPC records provide a proximal reference for the concentration and diversity of Patagonian airborne particles subsequently transported across Antarctica and the sub-Antarctic region (Gassó & Stein, 2007; Li et al., 2010; Tetzner, Allen, & Thomas, 2022).

CDB core data sets represent one of the few available in situ observations of snow accumulation in the CDI. Previous studies, using satellite-derived estimates, suggest that the upper section of the Marinelli glacier has been increasing in mass (Melkonian et al., 2013). However, the satellite derived snow accumulation is more than double the value estimated from our CDB core. This discrepancy could be explained by a combination of different data acquisition periods (2001–2011 (Melkonian et al., 2013) versus 2017–2020 (this study)), satellite-derived data biases, post-depositional processes, and the steep topography surrounding the confined CDB site. Despite the satellite-derived estimates identifying areas of snow accumulation which could be harvested for future ice core research, our ERA5-2000 and DOWN-2000 surface air temperature estimations suggest well-preserved ice core records are confined to the icefield's high elevation areas (>2,000 m a.s.l.).

Our results show a considerable increase in PDD estimates over the last decades, suggesting sites above 2,000 m of elevation have been progressively exposed to temperature induced melting conditions. Despite potential inaccuracies in summer surface air temperature estimations, PDD at ERA5-2000 and DOWN-2000 are disproportionately higher than ERA5-DRILL and DOWN-DRILL PDD (Figure 2). This large difference can be explained by higher temperatures at lower elevation, where mean surface air temperature exceeds the melting point for an extended period. Thus, while there is little evidence of significant melt at CDB, elevations below 2000 m are likely more vulnerable. This is consistent with evidence of significant melt at 1800 m elevation (Mayewski et al., 2016). Surface melting is known to influence the elution of chemical and isotopic species, which could risk the seasonal marker preservation. Soluble species are more susceptible to melt induced migration than non-soluble species, which are more stable (Moser et al., 2024). Thus, the non-soluble pollen, diatoms and MPC evaluated in this study provide promising seasonal markers for sites at risk of melt.

A longer core from this region could provide useful information to directly and/or indirectly reconstruct past environmental changes in the current core of the westerly wind belt. MPC, nssCa^{2+}, marine ions, and diatom records have the potential to be harvested for past wind proxies (Tetzner, Thomas, et al., 2022). However, a thorough assessment should be conducted on each parameter to validate the environmental controls of these proxies.

5. Conclusions

The CDI is located in a key position to record changes in the SHWW belt. In this study, we assessed the preservation of both soluble chemistry and insoluble microparticle records in the first firn core drilled from the CDI. Our study confirms firn layers are well-preserved at elevations >2,300 m a.s.l., with multiple, thin (<2 mm) crust-like features, but few thicker melt layers (>0.5 cm). Chemical impurities and insoluble microparticle records are largely locally sourced and appear to preserve regional seasonality. Conversely, the stable water isotope records lack of a clear seasonality, preventing their direct use to reconstruct local surface air temperatures. Surface air temperature estimates are useful to assess current CDB site exposure to snow melt conditions, but largely based on uncertain regional lapse rate values. Based on our surface air temperature estimations, we propose the 2,000 m elevation contour as a threshold for the reliable preservation of paleoenvironmental information in the CDI firn. Future research should be focused on (a) conducting long radiosonde monitoring campaigns, aiming to improve regional lapse rate estimates (b) calibrating the environmental proxies preserved in the Cordillera Darwin ice core record and, (c) investigating the development and frequency of thin ice features likely caused by wind erosion and potentially disrupting the CDB record.

Conflict of Interest

The authors declare no conflicts of interest relevant to this study.

Data Availability Statement

The data sets original to this work can be found in Tetzner, Thomas, et al. (2025) and Tetzner, Temme, and Furst (2025), published at the UK Polar Data Centre.

Acknowledgments

We would like to thank Iris Buisman and Giulio Lampronti from the Microscopy Lab, Earth Sciences Department, University of Cambridge, for their technical support in the use of the SEM. We want to thank the two anonymous reviewers for their constructive comments that led to an improved manuscript. We would like to thank Cristian Donoso and Cristóbal Clement for allowing us to use their Cordillera Darwin image (Figure 1c). We would like to thank the Corporacion Nacional Forestal—Magallanes (CONAF Magallanes) for granting us permits to conduct fieldwork activities in the Alberto de Agostini National Park, Chile. This research was funded by Dieter Tetzner's National Geographic Early Career Grant 2019. FT was funded by the German Research Foundation (DFG) within the MAGIC project (FU 1032/5-1) and the RESPONSE project (TA 1719/2-1). JJF has received funding from the European Union's Horizon 2020 research and innovation programme via the European Research Council (ERC) as a Starting Grant (StG) under Grant agreement no 948290.

References

Adame, J. A., Cupeiro, M., Yela, M., Cuevas, E., & Carbajal, G. (2019). Ozone and carbon monoxide at the Ushuaia GAW-WMO global station. *Atmospheric Research*, *217*, 1–9. https://doi.org/10.1016/j.atmosres.2018.10.015

Alley, R. B. (2010). Reliability of ice-core science: Historical insights. *Journal of Glaciology*, *56*(200), 1095–1103. https://doi.org/10.3189/002214311796406130

Almandoz, G. O., Hernando, M. P., Ferreyra, G. A., Schloss, I. R., & Ferrario, M. E. (2011). Seasonal phytoplankton dynamics in extreme southern South America (Beagle channel, Argentina). *Journal of Sea Research*, *66*(2), 47–57. https://doi.org/10.1016/j.seares.2011.03.005

Aristarain, A. J., & Delmas, R. J. (1993). Firn-core study from the southern Patagonia ice cap, South America. *Journal of Glaciology*, *39*(132), 249–254. https://doi.org/10.3189/s0022143000015914

Bagmet, V. B., Abdullin, S. R., Nikulin, A. Y., Nikulin, V. Y., & Gontcharov, A. A. (2022). Biology, genetic diversity, and ecology of Nitzschia acidoclinata Lange-Bertalot (Bacillariophyta). *Diversity*, *14*(12), 1133. https://doi.org/10.3390/d14121133

Barrera, M. D., Frangi, J. L., Richter, L. L., Perdomo, M. H., & Pinedo, L. B. (2000). Structural and functional changes in Nothofagus pumilio forests along an altitudinal gradient in Tierra del Fuego, Argentina. *Journal of Vegetation Science*, *11*(2), 179–188. https://doi.org/10.2307/3236797

Björck, S., Rundgren, M., Ljung, K., Unkel, I., & Wallin, Å. (2012). Multi-proxy analyses of a peat bog on Isla de los Estados, easternmost Tierra del Fuego: A unique record of the variable Southern Hemisphere Westerlies since the last deglaciation. *Quaternary Science Reviews*, *42*, 1–14. https://doi.org/10.1016/j.quascirev.2012.03.015

Bowen, H. J. M. (1979). *Environmental chemistry of the elements*. Academic Press.

Bown, F., Rivera, A., Pętlicki, M., Bravo, C., Oberreuter, J., & Moffat, C. (2019). Recent ice dynamics and mass balance of Jorge Montt glacier, southern Patagonia icefield. *Journal of Glaciology*, *65*(253), 732–744. https://doi.org/10.1017/jog.2019.47

Brönnimann, S., Mariani, I., Schwikowski, M., Auchmann, R., & Eichler, A. (2013). Simulating the temperature and precipitation signal in an Alpine ice core. *Climate of the Past*, *9*(4), 2013–2022. https://doi.org/10.5194/cp-9-2013-2013

Buttstädt, M., Möller, M., Iturraspe, R., & Schneider, C. (2009). Mass balance evolution of Martial Este Glacier, Tierra del Fuego (Argentina) for the period 1960–2099. *Advances in Geosciences*, *22*, 117–124. https://doi.org/10.5194/adgeo-22-117-2009

Cai, W., & Cowan, T. (2007). Trends in Southern Hemisphere circulation in IPCC AR4 models over 1950–99: Ozone depletion versus greenhouse forcing. *Journal of Climate*, *20*(4), 681–693. https://doi.org/10.1175/jcli4028.1

Carrasco, J. F., Casassa, G., & Rivera, A. (2002). Meteorological and climatological aspects of the southern Patagonia icefield. In *The Patagonian icefields: A unique natural laboratory for environmental and climate change studies* (pp. 29–41). Springer US.

Carrivick, J. L., Davies, B. J., James, W. H., Quincey, D. J., & Glasser, N. F. (2016). Distributed ice thickness and glacier volume in southern South America. *Global and Planetary Change*, *146*, 122–132. https://doi.org/10.1016/j.gloplacha.2016.09.010

Casado, M., Landais, A., Picard, G., Arnaud, L., Dreossi, G., Stenni, B., & Prié, F. (2021). Water isotopic signature of surface snow metamorphism in Antarctica. *Geophysical Research Letters*, *48*(17), e2021GL093382. https://doi.org/10.1029/2021gl093382

Casado, M., Landais, A., Picard, G., Münch, T., Laepple, T., Stenni, B., et al. (2018). Archival processes of the water stable isotope signal in East Antarctic ice cores. *The Cryosphere*, *12*(5), 1745–1766. https://doi.org/10.5194/tc-12-1745-2018

Casado, M., Münch, T., & Laepple, T. (2020). Climatic information archived in ice cores: Impact of intermittency and diffusion on the recorded isotopic signal in Antarctica. *Climate of the Past*, *16*(4), 1581–1598. https://doi.org/10.5194/cp-16-1581-2020

Cefarelli, A. O., Ferrario, M. E., Almandoz, G. O., Atencio, A. G., Akselman, R., & Vernet, M. (2010). Diversity of the diatom genus Fragilariopsis in the Argentine sea and Antarctic waters: Morphology, distribution and abundance. *Polar Biology*, *33*(11), 1463–1484. https://doi.org/10.1007/s00300-010-0794-z

Ciniglia, C., Cennamo, P., De Stefano, M., Pinto, G., Caputo, P., & Pollio, A. (2007). Pinnularia obscura Krasske (Bacillariophyceae, Bacillariophyta) from acidic environments: Characterization and comparison with other acid-tolerant Pinnularia species. *Fundamental and applied limnology*, *170*(1), 29–47. https://doi.org/10.1127/1863-9135/2007/0170-0029

Cogley, J. G., Arendt, A. A., Bauder, A., Braithwaite, R. J., Hock, R., Jansson, P., & Zemp, M. (2010). Glossary of glacier mass balance and related terms.

Cosentino, N. J., Gaiero, D. M., & Lambert, F. (2021). Present-day patagonian dust emissions: Combining surface visibility, mass flux, and reanalysis data. *Journal of Geophysical Research: Atmospheres*, *126*(16), e2020JD034459. https://doi.org/10.1029/2020jd034459

Cosentino, N. J., Ruiz-Etcheverry, L. A., Bia, G. L., Simonella, L. E., Coppo, R., Torre, G., et al. (2020). Does satellite chlorophyll-a respond to southernmost Patagonian dust? A multi-year, event-based approach. *Journal of Geophysical Research: Biogeosciences*, *125*(12), e2020JG006073. https://doi.org/10.1029/2020jg006073

Dansgaard, W. (1964). Stable isotopes in precipitation. *Tellus*, *16*(4), 436–468. https://doi.org/10.3402/tellusa.v16i4.8993

Deng, K., Azorin-Molina, C., Yang, S., Hu, C., Zhang, G., Minola, L., & Chen, D. (2022). Changes of Southern Hemisphere westerlies in the future warming climate. *Atmospheric Research*, *270*, 106040. https://doi.org/10.1016/j.atmosres.2022.106040

Deppeler, S. L., & Davidson, A. T. (2017). Southern Ocean phytoplankton in a changing climate. *Frontiers in Marine Science*, *4*, 40. https://doi.org/10.3389/fmars.2017.00040

Draxler, R. R., & Hess, G. D. (1998). An overview of the HYSPLIT_4 modelling system for trajectories. *Australian Meteorological Magazine*, *47*(4), 295–308.

Ekaykin, A. A., Lipenkov, V. Y., Barkov, N. I., Petit, J. R., & Masson-Delmotte, V. (2002). Spatial and temporal variability in isotope composition of recent snow in the vicinity of Vostok station, Antarctica: Implications for ice-core record interpretation. *Annals of Glaciology*, *35*, 181–186. https://doi.org/10.3189/172756402781816726

Espinosa, M. A. (2008). Diatoms from Patagonia and Tierra del Fuego. *Developments in Quaternary Science*, *11*, 383–392. https://doi.org/10.1016/s1571-0866(07)10019-1

Farnsworth, A., Valdes, P. J., Spicer, R. A., Ding, L., Witkowski, C., Lauretano, V., et al. (2021). Paleoclimate model-derived thermal lapse rates: Towards increasing precision in paleoaltimetry studies. *Earth and Planetary Science Letters*, *564*, 116903. https://doi.org/10.1016/j.epsl.2021.116903

Fernandoy, F., Tetzner, D., Meyer, H., Gacitúa, G., Hoffmann, K., Falk, U., et al. (2018). New insights into the use of stable water isotopes at the northern Antarctic Peninsula as a tool for regional climate studies. *The Cryosphere*, *12*(3), 1069–1090. https://doi.org/10.5194/tc-12-1069-2018

Flores-Melo, X., Giesecke, R., Schloss, I. R., Latorre, M. P., De Madron, X. D., Bourrin, F., et al. (2024). Seasonal and spatial variability of vertical particle flux along the Beagle Channel (Southern Patagonia). *Journal of Marine Systems*, *241*, 103913. https://doi.org/10.1016/j.jmarsys.2023.103913

Fogt, R. L., & Marshall, G. J. (2020). The southern annular mode: Variability, trends, and climate impacts across the southern Hemisphere. *Wiley Interdisciplinary Reviews: Climate Change*, *11*(4), e652. https://doi.org/10.1002/wcc.652

Gassó, S., & Stein, A. F. (2007). Does dust from Patagonia reach the sub-Antarctic Atlantic Ocean? *Geophysical Research Letters*, *34*(1). https://doi.org/10.1029/2006gl027693

Gillett, N. P., & Thompson, D. W. (2003). Simulation of recent Southern Hemisphere climate change. *Science*, *302*(5643), 273–275. https://doi.org/10.1126/science.1087440

Gkinis, V., Holme, C., Kahle, E. C., Stevens, M. C., Steig, E. J., & Vinther, B. M. (2021). Numerical experiments on firn isotope diffusion with the Community Firn Model. *Journal of Glaciology*, *67*(263), 450–472. https://doi.org/10.1017/jog.2021.1

Gong, X., Radenz, M., Wex, H., Seifert, P., Ataei, F., Henning, S., et al. (2022). Significant continental source of ice-nucleating particles at the tip of Chile's southernmost Patagonia region. *Atmospheric Chemistry and Physics*, *22*(16), 10505–10525. https://doi.org/10.5194/acp-22-10505-2022

González-Reyes, Á., Jacques-Coper, M., Bravo, C., Rojas, M., & Garreaud, R. (2023). Evolution of heatwaves in Chile since 1980. *Weather and Climate Extremes*, *41*, 100588. https://doi.org/10.1016/j.wace.2023.100588

Gorodetskaya, I. V., Durán-Alarcón, C., González-Herrero, S., Clem, K. R., Zou, X., Rowe, P., et al. (2023). Record-high Antarctic Peninsula temperatures and surface melt in February 2022: A compound event with an intense atmospheric river. *npj climate and atmospheric science*, *6*(1), 202. https://doi.org/10.1038/s41612-023-00529-6

Goursaud, S., Masson-Delmotte, V., Favier, V., Preunkert, S., Legrand, M., Minster, B., & Werner, M. (2019). Challenges associated with the climatic interpretation of water stable isotope records from a highly resolved firn core from Adélie Land, coastal Antarctica. *The Cryosphere*, *13*(4), 1297–1324. https://doi.org/10.5194/tc-13-1297-2019

Grieman, M. M., Hoffmann, H. M., Humby, J. D., Mulvaney, R., Nehrbass-Ahles, C., Rix, J., et al. (2022). Continuous flow analysis methods for sodium, magnesium and calcium detection in the Skytrain ice core. *Journal of Glaciology*, *68*(267), 90–100. https://doi.org/10.1017/jog.2021.75

Grigholm, B., Mayewski, P. A., Kurbatov, A. V., Casassa, G., Staeding, A. C., Handley, M., et al. (2009). Chemical composition of fresh snow from Glaciar Marinelli, Tierra del Fuego, Chile. *Journal of Glaciology*, *55*(193), 769–776. https://doi.org/10.3189/002214309790152546

Hall, B. L., Porter, C. T., Denton, G. H., Lowell, T. V., & Bromley, G. R. (2013). Extensive recession of Cordillera Darwin glaciers in southernmost South America during Heinrich stadial 1. *Quaternary Science Reviews*, *62*, 49–55. https://doi.org/10.1016/j.quascirev.2012.11.026

Hasle, G. R., & Syvertsen, E. E. (1997). Chapter 2 – Marine diatoms. In C. R. Tomas (Ed.), *Identifying marine Phytoplankton* (pp. 5–385). Academic Press. https://doi.org/10.1016/B978-012693018-4/50004-5

Hassett, M. O., Fischer, M. W., & Money, N. P. (2015). Mushrooms as rainmakers: How spores act as nuclei for raindrops. *PLoS One*, *10*(10), e0140407. https://doi.org/10.1371/journal.pone.0140407

Hechenleitner, P., Gardner, M. F., Thomas, P. I., Echeverría, C., Escobar, B., Brownless, P., & Martínez, C. (2005). Plantas amenazas del Centro-Sur de Chile: Distribución, Conservación y Propagación. *Universidad Austral de Chile y Real Jardın Botanico de Edimburgo*.

Hedding, D. W. (2006). *Geomorphology and geomorphological responses to climate change in the interior of sub-Antarctic Marion Island*. University of Pretoria.
Hersbach, H., Bell, B., Berrisford, P., Hirahara, S., Horányi, A., Muñoz-Sabater, J., et al. (2020). The ERA5 global reanalysis. *Quarterly Journal of the Royal Meteorological Society*, *146*(730), 1999–2049. https://doi.org/10.1002/qj.3803
Heusser, C. J. (1971). *Pollen and spores of Chile*. The University of Arizona Press.
Hoffmann-Abdi, K., Fernandoy, F., Meyer, H., Freitag, J., Opel, T., McConnell, J. R., & Schneider, C. (2023). Correction: Hoffmann-Abdi et al. Short-Term meteorological and environmental signals recorded in a firn core from a high-accumulation site on plateau Laclavere, Antarctic Peninsula. Geosciences 2021, 11, 428. *Geosciences*, *13*(8), 237. https://doi.org/10.3390/geosciences13080237
Holmlund, P., & Fuenzalida, H. (1995). Anomalous glacier responses to 20th century climatic changes in Darwin Cordillera, southern Chile. *Journal of Glaciology*, *41*(139), 465–473. https://doi.org/10.3189/s0022143000034808
Holz, A., & Veblen, T. T. (2011). Variability in the southern annular mode determines wildfire activity in Patagonia. *Geophysical Research Letters*, *38*(14). https://doi.org/10.1029/2011gl047674
Huber, C. J., Eichler, A., Mattea, E., Brütsch, S., Jenk, T. M., Gabrieli, J., et al. (2024). High-altitude glacier archives lost due to climate change-related melting. *Nature Geoscience*, *17*(2), 1–4. https://doi.org/10.1038/s41561-023-01366-1
Hutton, J. T. (1977). Sodium and chloride in rainwater. *Nature*, *268*(5620), 568. https://doi.org/10.1038/268568a0
Jiahong, W., Jiancheng, K., Jiankang, H., Zichu, X., Leibao, L., & Dali, W. (1998). Glaciological studies on the King George Island ice cap, south Shetland islands, Antarctica. *Annals of Glaciology*, *27*, 105–109. https://doi.org/10.3189/1998aog27-1-105-109
JiankANG, H. A. N., Zichu, X., Xinping, Z., Dongsheng, D., Mayewski, P. A., & Twickler, M. S. (2001). Methanesulfonate in the firn of King George Island, Antarctica. *Journal of Glaciology*, *47*(159), 589–594. https://doi.org/10.3189/172756501781831828
Kilian, R., & Lamy, F. (2012). A review of Glacial and Holocene paleoclimate records from southernmost Patagonia (49–55 S). *Quaternary Science Reviews*, *53*, 1–23. https://doi.org/10.1016/j.quascirev.2012.07.017
Kociolek, J. P., Kopalová, K., Hamsher, S. E., Kohler, T. J., Van de Vijver, B., Convey, P., & McKnight, D. M. (2017). Freshwater diatom biogeography and the genus Luticola: An extreme case of endemism in Antarctica. *Polar Biology*, *40*(6), 1185–1196. https://doi.org/10.1007/s00300-017-2090-7
Koerner, R. M. (1997). Some comments on climatic reconstructions from ice cores drilled in areas of high melt. *Journal of Glaciology*, *43*(143), 90–97. https://doi.org/10.3189/S0022143000002847
Kohshima, S., Shiraiwa, T., Godoi, M. A., Kubota, K., Takeuchi, N., & Shinbori, K. (2002). Ice core drilling on Southern Patagonia icefield-development of a new portable drill and the field expedition in 1999. *Memoirs of National Institute of Polar Research - Special Issue*, *56*, 49–58.
Krammer, K. (2000). The genus *Pinnularia*. In H. Lange-Bertalot (Ed.), *Diatoms of the European inland waters and comparable habitats* (Vol. 1, pp. 1–703). A.R.G. Gantner Verlag K.G.
Lavers, D. A., Simmons, A., Vamborg, F., & Rodwell, M. J. (2022). An evaluation of ERA5 precipitation for climate monitoring. *Quarterly Journal of the Royal Meteorological Society*, *148*(748), 3152–3165. https://doi.org/10.1002/qj.4351
Le Quéré, C., Rodenbeck, C., Buitenhuis, E. T., Conway, T. J., Langenfelds, R., Gomez, A., et al. (2007). Saturation of the Southern Ocean CO2 sink due to recent climate change. *Science*, *316*(5832), 1735–1738. https://doi.org/10.1126/science.1136188
Li, F., Ginoux, P., & Ramaswamy, V. (2010). Transport of Patagonian dust to Antarctica. *Journal of Geophysical Research*, *115*(D18). https://doi.org/10.1029/2009jd012356
Li, L., & Pomeroy, J. W. (1997). Estimates of threshold wind speeds for snow transport using meteorological data. *Journal of Applied Meteorology and Climatology*, *36*(3), 205–213. https://doi.org/10.1175/1520-0450(1997)036<0205:eotwsf>2.0.co;2
Liu, Z., Bao, Y., Thompson, L. G., Mosley-Thompson, E., Tabor, C., Zhang, G. J., et al. (2023). Tropical mountain ice core δ18O: A goldilocks indicator for global temperature change. *Science Advances*, *9*(45), eadi6725. https://doi.org/10.1126/sciadv.adi6725
Lorion, J., & Small, E. (2021). Crowberry (Empetrum): A chief Arctic traditional indigenous fruit in need of economic and ecological management. *The Botanical Review*, *87*(3), 259–310. https://doi.org/10.1007/s12229-021-09248-0
Lovenduski, N. S., Gruber, N., Doney, S. C., & Lima, I. D. (2007). Enhanced CO2 outgassing in the Southern Ocean from a positive phase of the southern annular mode. *Global Biogeochemical Cycles*, *21*(2). https://doi.org/10.1029/2006gb002900
Lowe, R. L. (1975). Comparative ultra structure of the valves of some Cyclotella species (bacillariophyceae). *Journal of Phycology*, *11*(4), 415–424. https://doi.org/10.1111/j.1529-8817.1975.tb02805.x
Lowe, R. L. (2003). Keeled and canalled raphid diatoms. In *Freshwater algae of north America* (pp. 669–684). Academic Press.
Mancini, M. V., de Porras, M. E., & Bamonte, F. P. (2012). Southernmost South America steppes: Vegetation and its modern pollen-assemblages representation. In D. Germanno (Ed.), *Steppe ecosystems: Dynamics, land use and conservation* (pp. 141–156). Nova Science Publishers, Inc.
Markgraf, V., & Huber, U. M. (2010). Late and postglacial vegetation and fire history in Southern Patagonia and Tierra del Fuego. *Palaeogeography, Palaeoclimatology, Palaeoecology*, *297*(2), 351–366. https://doi.org/10.1016/j.palaeo.2010.08.013
Markle, B. R., & Steig, E. J. (2022). Improving temperature reconstructions from ice-core water-isotope records. *Climate of the Past*, *18*(6), 1321–1368. https://doi.org/10.5194/cp-18-1321-2022
Marshall, G. J. (2003). Trends in the southern annular mode from observations and reanalyses. *Journal of Climate*, *16*(24), 4134–4143. https://doi.org/10.1175/1520-0442(2003)016<4134:titsam>2.0.co;2
Marshall, G. J., Thompson, D. W., & van den Broeke, M. R. (2017). The signature of Southern Hemisphere atmospheric circulation patterns in Antarctic precipitation. *Geophysical Research Letters*, *44*(22), 11–580. https://doi.org/10.1002/2017gl075998
Matsuoka, K., & Naruse, R. (1999). Mass balance features derived from a firn core at Hielo Patagonico Norte, South America. *Arctic Antarctic and Alpine Research*, *31*(4), 333–340. https://doi.org/10.1080/15230430.1999.12003318
Mayewski, P. A., Kuli, A., Casassa, G., Arévalo, M., Dixon, D. A., Grigholm, B., et al. (2016). Initial reconnaissance for a South Georgia ice core. *Journal of Glaciology*, *62*(231), 54–61. https://doi.org/10.1017/jog.2016.9
McCulloch, R. D., Mathiasen, P., & Premoli, A. C. (2022). Palaeoecological evidence of pollen morphological changes: A climate change adaptation strategy? *Palaeogeography, Palaeoclimatology, Palaeoecology*, *601*, 111157. https://doi.org/10.1016/j.palaeo.2022.111157
Melkonian, A. K., Willis, M. J., Pritchard, M. E., Rivera, A., Bown, F., & Bernstein, S. A. (2013). Satellite-derived volume loss rates and glacier speeds for the Cordillera Darwin Icefield, Chile. *The Cryosphere*, *7*(3), 823–839. https://doi.org/10.5194/tc-7-823-2013
Minowa, M., Skvarca, P., & Fujita, K. (2023). Climate and surface mass balance at Glaciar Perito Moreno, southern Patagonia. *Journal of Climate*, *36*(2), 625–641. https://doi.org/10.1175/jcli-d-22-0294.1
Möller, M., Schneider, C., & Kilian, R. (2007). Glacier change and climate forcing in recent decades at Gran Campo Nevado, southernmost Patagonia. *Annals of Glaciology*, *46*, 136–144. https://doi.org/10.3189/172756407782871530
Moore, P. D., Webb, J. A., & Collinson, M. E. (1991). *Pollen analysis*. Blackwell Scientific.

Moreno, P. I., Vilanova, I., Villa-Martínez, R., Garreaud, R. D., Rojas, M., & De Pol-Holz, R. (2014). Southern Annular Mode-like changes in southwestern Patagonia at centennial timescales over the last three millennia. *Nature Communications*, *5*(1), 1–7.

Moreno, P. I., Villa-Martínez, R., Cárdenas, M. L., & Sagredo, E. A. (2012). Deglacial changes of the southern margin of the southern westerly winds revealed by terrestrial records from SW Patagonia (52 S). *Quaternary Science Reviews*, *41*, 1–21. https://doi.org/10.1016/j.quascirev.2012.02.002

Moser, D. E., Jackson, S., Kjær, H. A., Markle, B., Ngoumtsa, E., Pedro, J. B., et al. (2021). An age scale for the first shallow (sub-) Antarctic ice core from Young Island, Northwest Ross Sea. *Geosciences*, *11*(9), 368. https://doi.org/10.3390/geosciences11090368

Moser, D. E., Thomas, E. R., Nehrbass-Ahles, C., Eichler, A., & Wolff, E. (2024). Melt-affected ice cores for polar research in a warming world. *The Cryosphere*, *18*(6), 2691–2718. https://doi.org/10.5194/tc-18-2691-2024

Musotto, L. L., Borromei, A. M., Bianchinotti, M. V., Coronato, A., Menounos, B., Osborn, G., & Marr, R. (2017). Postglacial environments in the southern coast of Lago Fagnano, central Tierra del Fuego, Argentina, based on pollen and fungal microfossils analyses. *Review of Palaeobotany and Palynology*, *238*, 43–54. https://doi.org/10.1016/j.revpalbo.2016.11.016

Nye, J. F. (1963). Correction factor for accumulation measured by the thickness of the annual layers in an ice sheet. *Journal of Glaciology*, *4*(36), 785–788. https://doi.org/10.3189/s0022143000028367

Oliver, J. E. (2005). Maritime climate. Encyclopedia of world climatology. *Encyclopedia of Earth Sciences Series*, 477–479.

Orsi, A. J., Kawamura, K., Fegyveresi, J. M., Headly, M. A., Alley, R. B., & Severinghaus, J. P. (2015). Differentiating bubble-free layers from melt layers in ice cores using noble gases. *Journal of Glaciology*, *61*(227), 585–594. https://doi.org/10.3189/2015jog14j237

Ovadnevaite, J., Ceburnis, D., Canagaratna, M., Berresheim, H., Bialek, J., Martucci, G., et al. (2012). On the effect of wind speed on submicron sea salt mass concentrations and source fluxes. *Journal of Geophysical Research*, *117*(D16). https://doi.org/10.1029/2011jd017379

Pfahl, S., & Sodemann, H. (2014). What controls deuterium excess in global precipitation? *Climate of the Past*, *10*(2), 771–781. https://doi.org/10.5194/cp-10-771-2014

Pinseel, E., Janssens, S. B., Verleyen, E., Vanormelingen, P., Kohler, T. J., Biersma, E. M., et al. (2020). Global radiation in a rare biosphere soil diatom. *Nature Communications*, *11*(1), 2382. https://doi.org/10.1038/s41467-020-16181-0

Pitman, Z. (2023). Evaluating Snow and Ice Cover in Tierra del Fuego, Argentina. *Geosciences Undergraduate Honors Theses*. Retrieved from https://scholarworks.uark.edu/geosuht/3

Polvani, L. M., Waugh, D. W., Correa, G. J., & Son, S. W. (2011). Stratospheric ozone depletion: The main driver of twentieth-century atmospheric circulation changes in the Southern Hemisphere. *Journal of Climate*, *24*(3), 795–812. https://doi.org/10.1175/2010jcli3772.1

Reis, R. S. D., da Rocha Ribeiro, R., Delmonte, B., Ramirez, E., Dani, N., Mayewski, P. A., & Simões, J. C. (2022). The recent relationships between Andean ice-core dust record and Madeira river suspended sediments on the wet season. *Frontiers in Environmental Science*, *10*, 840884. https://doi.org/10.3389/fenvs.2022.840884

Rumrich, U., Lange-Bertalot, H., & Rumrich, M. (2000). Diatoms of the Andes. From Venezuela to Patagonia/Tierra del Fuego. In H. Lange-Bertalot (Ed.), *Iconographia Diatomologica. Annotated diatom Micrographs. Vol. 9. Phytogeography-Diversity-Taxonomy* (Vol. 9, p. 673). Koeltz Scientific Books.

Russell, J. L., Dixon, K. W., Gnanadesikan, A., Stouffer, R. J., & Toggweiler, A. (2006). The Southern Hemisphere westerlies in a warming world: Propping open the door to the deep ocean. *Journal of Climate*, *19*(24), 6382–6390. https://doi.org/10.1175/jcli3984.1

Schneider, C., Glaser, M., Kilian, R., Santana, A., Butorovic, N., & Casassa, G. (2003). Weather observations across the southern Andes at 53°S. *Physical Geography*, *24*(2), 97–119. https://doi.org/10.2747/0272-3646.24.2.97

Schwikowski, M., Brütsch, S., Casassa, G., & Rivera, A. (2006). A potential high-elevation ice-core site at Hielo Patagónico Sur. *Annals of Glaciology*, *43*, 8–13. https://doi.org/10.3189/172756406781812014

Schwikowski, M., Schläppi, M., Santibañez, P., Rivera, A., & Casassa, G. (2013). Net accumulation rates derived from ice core stable isotope records of Pío XI glacier, Southern Patagonia Icefield. *The Cryosphere*, *7*(5), 1635–1644.

Shumilovskikh, L. S., & van Geel, B. (2020). Non-pollen Palynomorphs. In A. G. Henry (Ed.), *Handbook for the analysis of micro-particles in archaeological samples* (pp. 65–94). Springer.

Simões, J. C., Ferron, F. A., Bernardo, R. T., Aristarain, A. J., Stiévenard, M. I. C. H. E. L., Pourchet, M. I. C. H. E. L., & Delmas, R. J. (2004). Ice core study from the King George Island, south Shetlands, Antarctica. *Pesquisa Antártica Brasileira*, *4*(9–23), 9–23. https://doi.org/10.31789/pab.v4n1.002

Simonato, J., Sala, S., Vouilloud, A., Lamaro, A., & Kociolek, J. P. (2017). Distribución de los taxones del género Luticola mencionados por J. Frenguelli en Argentina y Antártida. Retrieved from http://sedici.unlp.edu.ar/handle/10915/180381

Son, S. W., Polvani, L. M., Waugh, D. W., Akiyoshi, H., Garcia, R., Kinnison, D., et al. (2008). The impact of stratospheric ozone recovery on the Southern Hemisphere westerly jet. *Science*, *320*(5882), 1486–1489. https://doi.org/10.1126/science.1155939

Stein, A. F., Draxler, R. R., Rolph, G. D., Stunder, B. J., Cohen, M. D., & Ngan, F. (2015). NOAA's HYSPLIT atmospheric transport and dispersion modeling system. *Bulletin of the American Meteorological Society*, *96*(12), 2059–2077. https://doi.org/10.1175/bams-d-14-00110.1

Stillman, D. E., MacGregor, J. A., & Grimm, R. E. (2013). The role of acids in electrical conduction through ice. *Journal of Geophysical Research: Earth Surface*, *118*(1), 1–16. https://doi.org/10.1029/2012jf002603

Temme, F., Farías-Barahona, D., Seehaus, T., Jaña, R., Arigony-Neto, J., Gonzalez, I., et al. (2023). Strategies for regional modeling of surface mass balance at the Monte Sarmiento Massif, Tierra del Fuego. *The Cryosphere*, *17*(6), 2343–2365. https://doi.org/10.5194/tc-17-2343-2023

Tetzner, D., Temme, F., & Furst, J. (2025). ERA5 daily downscaled surface air temperature and snowfall at two Cordillera Darwin high elevation sites 2000 - 2022 CE (Version 1.0) [Dataset]. *NERC EDS UK Polar Data Centre*. https://doi.org/10.5285/eddc907c-f8e9-48c4-9f23-de0f674dbee0

Tetzner, D., Thomas, E., & Allen, C. (2019). A validation of ERA5 reanalysis data in the southern Antarctic Peninsula—Ellsworth land region, and its implications for ice core studies. *Geosciences*, *9*(7), 289. https://doi.org/10.3390/geosciences9070289

Tetzner, D., Thomas, E., Allen, C., McCulloch, R., Perren, B., McGuire, A., et al. (2025). Major ions, Stable water isotopes, Microparticle (dust, diatoms, pollen and spores) and electrical conductivity records from the first Cordillera Darwin ice core 2017 - 2020 CE (Version 1.0) [Dataset]. *NERC EDS UK Polar Data Centre*. https://doi.org/10.5285/2d9b5828-45d2-4361-b23b-cf027c15e97c

Tetzner, D., Thomas, E. R., Allen, C. S., & Wolff, E. W. (2021). A refined method to analyze insoluble particulate matter in ice cores, and its application to diatom sampling in the Antarctic Peninsula. *Frontiers in Earth Science*, *9*, 20. https://doi.org/10.3389/feart.2021.617043

Tetzner, D. R., Allen, C. S., & Thomas, E. R. (2022). Regional variability of diatoms in ice cores from the Antarctic Peninsula and Ellsworth land, Antarctica. *The Cryosphere*, *16*(3), 779–798. https://doi.org/10.5194/tc-16-779-2022

Tetzner, D. R., Thomas, E. R., Allen, C. S., & Grieman, M. M. (2022). Regional validation of the use of diatoms in ice cores from the Antarctic Peninsula as a Southern Hemisphere westerly wind proxy. *Climate of the Past*, *18*(7), 1709–1727. https://doi.org/10.5194/cp-18-1709-2022

Thomas, E. R., & Bracegirdle, T. J. (2009). Improving ice core interpretation using in situ and reanalysis data. *Journal of Geophysical Research*, *114*(D20). https://doi.org/10.1029/2009jd012263

Thomas, E. R., Gacitúa, G., Pedro, J. B., Faith King, A. C., Markle, B., Potocki, M., & Moser, D. E. (2021). Physical properties of shallow ice cores from Antarctic and sub-Antarctic islands. *The Cryosphere*, *15*(2), 1173–1186. https://doi.org/10.5194/tc-15-1173-2021

Thompson, L. G., Hastenrath, S., & Arnao, B. M. (1979). Climatic ice core records from the tropical Quelccaya ice cap. *Science*, *203*(4386), 1240–1243. https://doi.org/10.1126/science.203.4386.1240

Thompson, L. G., Mosley-Thompson, E., Davis, M. E., Lin, P. N., Henderson, K. A., Cole-Dai, J., et al. (1995). Late glacial stage and Holocene tropical ice core records from Huascaran, Peru. *Science*, *269*(5220), 46–50. https://doi.org/10.1126/science.269.5220.46

Toro Manríquez, M., Mestre, L., Lencinas, M. V., Promis, Á., Martínez Pastur, G., & Soler, R. (2016). Flowering and seeding patterns in pure and mixed Nothofagus forests in Southern Patagonia. *Ecological Processes*, *5*, 1–12.

Toro-Manríquez, M. D., Herrera, A. H., Soler, R. M., Lencinas, M. V., & Pastur, G. J. M. (2023). Combined effects of tree canopy composition, landscape location, and growing season on Nothofagus forest seeding patterns in Southern Patagonia. *Forest Ecology and Management*, *529*, 120708. https://doi.org/10.1016/j.foreco.2022.120708

Van Daele, M., Bertrand, S., Meyer, I., Moernaut, J., Vandoorne, W., Siani, G., et al. (2016). Late Quaternary evolution of Lago Castor (Chile, 45.6 S): Timing of the deglaciation in northern Patagonia and evolution of the southern westerlies during the last 17 kyr. *Quaternary Science Reviews*, *133*, 130–146. https://doi.org/10.1016/j.quascirev.2015.12.021

Vidal, O., Rosenfeld, G., Santin, J., Latorre, J., Muñoz-Arriagada, R., & Fernández, A. (2023). Flora de la Reserva Natural Pingüino Rey (Tierra del Fuego, Chile): Criterios y narrativas para la selección de plantas carismáticas. *Gayana. Botánica*, *80*(1), 1–15. https://doi.org/10.4067/s0717-66432023000100001

Vimeux, F., de Angelis, M., Ginot, P., Magand, O., Casassa, G., Pouyaud, B., et al. (2008). A promising location in Patagonia for paleoclimate and paleoenvironmental reconstructions revealed by a shallow firn core from Monte San Valentín (Northern Patagonia Icefield, Chile). *Journal of Geophysical Research*, *113*(D16). https://doi.org/10.1029/2007jd009502

Voordendag, A., Goger, B., Prinz, R., Sauter, T., Mölg, T., Saigger, M., & Kaser, G. (2024). A novel framework to investigate wind-driven snow redistribution over an Alpine glacier: Combination of high-resolution terrestrial laser scans and large-eddy simulations. *The Cryosphere*, *18*(2), 849–868. https://doi.org/10.5194/tc-18-849-2024

Wachter, P., Beck, C., Philipp, A., Höppner, K., & Jacobeit, J. (2020). Spatiotemporal variability of the southern annular mode and its influence on Antarctic surface temperatures. *Journal of Geophysical Research: Atmospheres*, *125*(23), e2020JD033818. https://doi.org/10.1029/2020jd033818

Wingenroth, M., & Heusser, C. J. (1984). *Pollen of the high Andean Flora. Quebrada Benjamin Matienzo, Province of Mendoza Argentina*. Instituto Argentino de Nivologia y Glaciologia.

Xia, Z., Yu, Z., & Loisel, J. (2018). Centennial-scale dynamics of the southern Hemisphere westerly winds across the Drake passage over the past two millennia. *Geology*, *46*(10), 855–858. https://doi.org/10.1130/g40187.1

Yamada, T. (1987). Glaciological characteristics revealed by 37.6-m deep core drilled at the accumulation area of San Rafael Glacier, the Northern Patagonia Icefield. *Bulletin of Glacier Research*, *4*, 59–67.